

Trace elements in sulfides from the Maozu Pb-Zn deposit, Yunnan Province, China: Implications for trace-element incorporation mechanisms and ore genesis

ZHENLI LI^{1,2}, LIN YE^{1,*}, YUSI HU^{1,2}, CHEN WEI^{1,2}, ZHILONG HUANG¹, YULONG YANG³, AND LEONID DANYUSHEVSKY⁴

¹State Key Laboratory of Ore Deposit Geochemistry, Institute of Geochemistry, Chinese Academy of Sciences, Guiyang 550081, China

²University of Chinese Academy of Sciences, Beijing, 100049, China

³College of Earth Sciences, Chengdu University of Technology, Chengdu 610059, China

⁴CODES, University of Tasmania, Hobart, Tasmania 7001, Australia

ABSTRACT

The Sichuan-Yunnan-Guizhou Pb-Zn metallogenic province (SYGMP) is an important region for Pb-Zn resources in China. However, considerable controversy remains as to whether the Pb-Zn deposits are Mississippi Valley Type (MVT). The Maozu deposit, a typical example of the carbonate-hosted Pb-Zn deposits in the SYGMP, occurs in the late Ediacaran Dengying Formation and its ore bodies are divided into three types: lower layer (LL), vein layer (VL), and upper layer (UL) ore bodies based on their spatial relationship. In this study, laser ablation–inductively coupled plasma–mass spectrometry (LA-ICP-MS) was used to systematically analyze the trace-element compositions of sphalerite and galena in these three ore bodies. The results show that sphalerite is characterized by Cd and Ge enrichment; Fe, Mn, and Co depletion; and local In and Sn enrichment. Most of these elements likely appear as solid solutions in sphalerite and show a wide compositional variation, which is probably related to the medium- and low-temperature mixing of the ore-forming fluids. The local enrichment of In and Sn is likely attributed to the long-distance migration of ore-forming fluids through In-Sn-bearing volcanoclastic rocks. In vs. Sn and (Cu + Sb) vs. (Ag + Ge) show strong correlations and similar element distribution in the mapped images, indicating that these elements may be incorporated into sphalerite via a coupled substitution for Zn as $2\text{In}^{3+} + \text{Sn}^{4+} + 2\Box \leftrightarrow 5\text{Zn}^{2+}$ (\Box = vacancies) and $4(\text{Cu}^+ + \text{Sb}^{3+}) + (\text{Ge}^{4+} + 2\text{Ag}^+) + 2\Box \leftrightarrow 13\text{Zn}^{2+}$. Galena is enriched in Ag and Sb with minor Cd and Se and depleted in Bi, and most of the elements may occur as solid solutions. Ag vs. Sb in galena displays a strong positive correlation, implying the coupled substitution of $\text{Ag}^+ + \text{Sb}^{3+} \leftrightarrow 2\text{Pb}^{2+}$. Notably, the majority of the trace-element concentrations gradually decrease in the order LL → UL except Fe, Co, Cu, and Ge, while Fe, In, and Sn in sphalerite and Ag and Sb in galena have the highest concentration in the VL, indicating that the VL is a secondary migration channel for the ore-forming fluids. Furthermore, the trace-element compositions of the sulfides in the Maozu Pb-Zn deposit are consistent with the typical MVT deposit (hosted in the carbonate sequence) but are markedly different from sedimentary exhalative (SEDEX), volcanogenic massive sulfide (VMS) and skarn-type deposits. Based on these results, as well as the geological and geochemical characteristics of the deposit, the Maozu Pb-Zn deposit is an MVT deposit.

Keywords: Maozu Pb-Zn deposit, sulfides, trace elements, LA-ICP-MS, mapping, MVT

INTRODUCTION

The Sichuan-Yunnan-Guizhou Pb-Zn metallogenic province (SYGMP), located in the southwestern margin of the Yangtze Block, China, is an important region of the South China giant low-temperature metallogenic domain and the major source of Pb-Zn-Ag-Ge in China (Hu and Zhou 2012; Zhou et al. 2013; Zhang et al. 2015; Ye et al. 2016). Approximately 400 Pb-Zn ore deposits and occurrences have been explored in the SYGMP (e.g., Zhang 2008; Wu 2013), most of which are hosted in the late Ediacaran to early Permian carbonate rocks; notably, late Ediacaran and Carboniferous carbonates are the principal host rocks (Wu 2013;

Ye et al. 2016). Previous studies have shown that all the Pb-Zn deposits in the SYGMP have striking epigenetic characteristics and share features with typical Mississippi Valley Type (MVT) deposits (Leach 1993, 2005) in terms of mineral assemblages, mineralization types, ore host rocks, and wall rock alterations. (e.g., Han et al. 2007; Zhang et al. 2015). However, the ore bodies of the Pb-Zn deposits in the SYGMP are typically characterized by massive, thick veinlets filling open spaces controlled by the structure of the host rock, with high grades of Pb and Zn at generally >20%, such as the Huize (Huang et al. 2004; Han et al. 2007), Maoping (Wei et al. 2015), and Fule (Zhu et al. 2016; Li et al. 2018a, 2018b) Pb-Zn deposits, which possess slightly different characteristics from those of typical MVT deposits (Leach 1993; Leach et al. 2005, 2006; Leach and Taylor 2009). Accordingly, the genetic types of these

* E-mail: yelin@vip.gyig.ac.cn. ORCID 0000-0002-2557-8314

Pb-Zn deposits in the SYGMP remain inconclusive (e.g., Huang et al. 2004; Zhou et al. 2013; Zhang et al. 2015; Li et al. 2018b). Several hypotheses for the ore genesis have been proposed in the past two decades, such as a distal magmatic-hydrothermal type related to a Permian Emeishan mantle plume (Xie 1963; Huang et al. 2004), a sedimentary reworked type (Liu and Lin 1999; Tu 1984), MVT (e.g., Zhang 2005; Li 2016; Li et al. 2018a; Wei et al. 2018a), and a unique Sichuan-Yunnan-Guizhou (SYG) type (Han et al. 2007; Zhou et al. 2013, 2018a, 2018b).

The Maozu deposit, a typical carbonate-hosted Pb-Zn deposit in the SYGMP, occurs in the Late Ediacaran Dengying Formation and has proven Pb + Zn reserves of ~2 Mt, with average grade of 4.15 wt% Pb and 7.25 wt% Zn (e.g., Liu 2009; Zhou et al. 2013; Li et al. 2018). Previous studies mainly focused on the geology (Liu and Lin 1999; He et al. 2006), metallogenic regularity (Chen 2002; Liu 2009; Liu and Zhang 2013) and source of the ore-forming metal (Zhou et al. 2013) in the deposit. Due to the lack of geochemical data, in particular the study of trace elements in sulfide, the ore genesis remains a subject of debate, although the following have been postulated: (1) sedimentary reworked type (Zhang 1984; Liu and Lin 1999; Zhang 2013); (2) SEDEX-type (Chen 2002; He et al. 2006); (3) SYG-type (Zhou et al. 2013); and (4) MVT (Liu 2009). These disparate classifications are confusing for ore deposit exploration and mining design.

Sphalerite, as the major mineral in Pb-Zn deposits, contains various useful elements such as Ga (Moskalyk 2003), Ge (Höll et al. 2007), In (Alfantazi and Moskalyk 2003), Cd (Bonnet et al. 2016), and Ag (Cook et al. 2009). Previous studies indicated that trace elements, such as Fe, Mn, Cd, Ge, In, Ga, Se, and Te, can be used to ascertain important genetic information and can, to a large extent, be used to classify ore genesis types (Zhang 1987; Cook et al. 2009; Ye et al. 2011, 2012, 2016; Li et al. 2016; Wei et al. 2018a, 2018b). The obvious limitation of bulk analysis of trace elements of sulfide separates is that a sample may include fine-grained sulfide minerals with complex texture from different origins, which is common in the Maozu deposit. By contrast, laser ablation-inductively coupled plasma-mass spectrometry (LA-ICP-MS) can accurately and effectively determine the sulfide trace-element concentrations of individual sulfide grains (e.g., Watling et al. 1995; Cook et al. 2009; Ye et al. 2011, 2016), making it possible to discriminate different stages in microscale sulfide grains (Cook et al. 2009; Ye et al. 2011, 2016; George et al. 2015, 2016). Furthermore, time-resolved LA-ICP-MS depth profiling can provide information on whether a given trace element is present within the sulfide matrix or enclosed as micro-inclusions, even for elements at extremely low concentrations (e.g., Cook et al. 2009; George et al. 2015; Bonnet et al. 2016).

In this study, to understand the distribution features and substitution mechanisms of the trace elements in the sulfides from the Maozu Pb-Zn deposit in Yunnan, China, LA-ICP-MS (spot and mapping analyses) was used to determine sphalerite and galena trace-element chemistry in the deposit. Combined with the geologic setting, these analyses contribute to the development of a robust deposit model.

GEOLOGY OF THE MAOZU Pb-ZN DEPOSIT

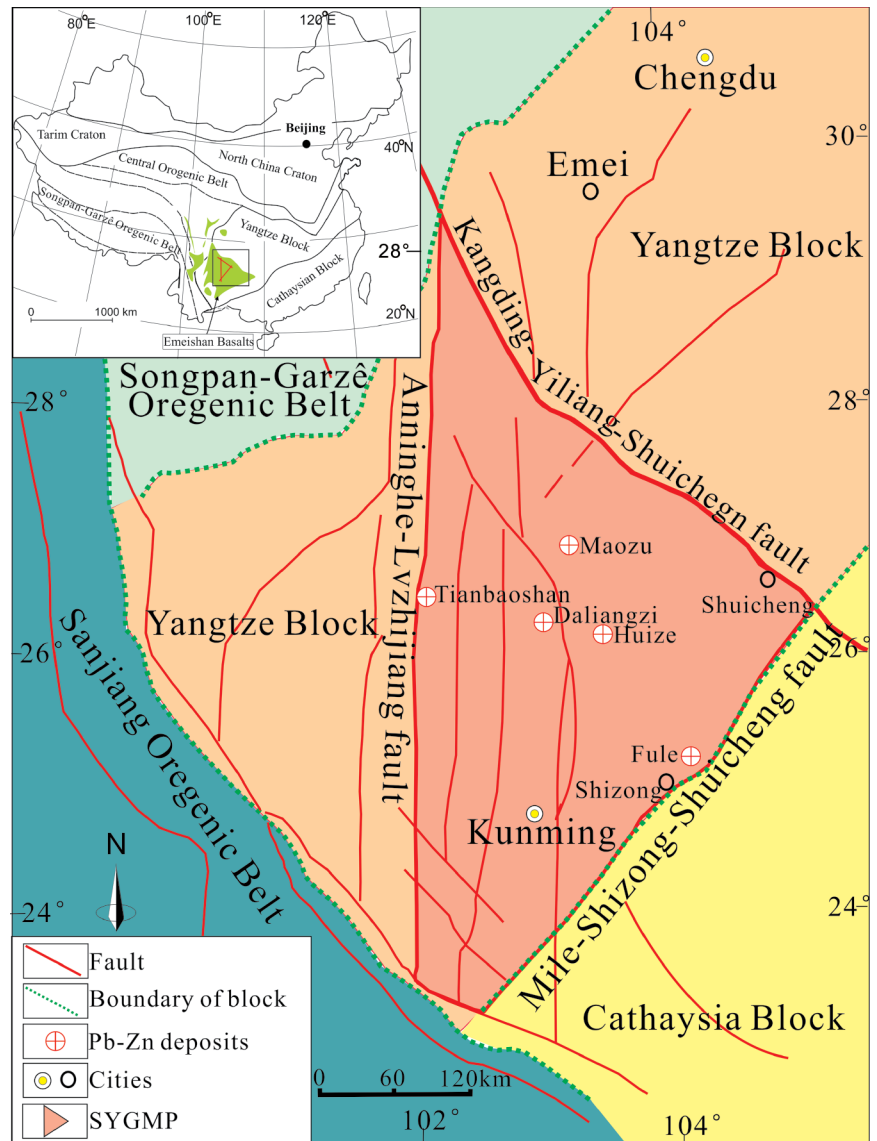
The Maozu Pb-Zn deposit is located in the western Yangtze block and northern SYGMP (Fig. 1). The SYGMP is an im-

portant production base of Pb, Zn, Ge, and Ag in China, and ~400 Pb-Zn deposits or occurrences (no economic value) have been found in the area. The exposed strata in the area include late Ediacaran to Quaternary strata (Fig. 2), including the late Ediacaran Dengying Formation, one of the chief ore-bearing strata in the region, which is mainly composed of phosphorus-bearing and silicified dolomite. The Cambrian strata consist of phosphorite, sandstone, and carbonate rocks. Ordovician strata are composed of sandy shale and argillaceous limestone. Silurian rocks are composed of siltstone and carbonates. The lower Devonian is mostly composed of sandstone and carbonates, and the upper Devonian is mainly composed of dolostone, which is one of the most important ore-hosting strata in the region. The Carboniferous strata are predominantly composed of (siliceous) carbonate rocks, which is another important ore-hosting strata in the region; for example, the world-class Huize Pb-Zn deposit mainly occurs in this Carboniferous strata. The Permian rocks predominantly consist of carbonates and basalts. The Triassic layer is mainly composed of clastic rocks and includes the main coal-bearing strata. The major composition of the Tertiary and Quaternary rocks is sediments that are exposed in the valley or river areas (Han et al. 2007). The north-south-striking faults and anticlines are well developed in this region (Zhang et al. 2006). The principal regional structures are the Anninghe-Lvzhijiang, Mile-Shizhong-Shuicheng, and Kangding-Yilian-Shuicheng tectonic belts (Fig. 1), most of which are regional compression thrust faults. The Permian Emeishan flood basalts are among the most widely distributed magmatic rocks in the area.

The Maozu deposit is a representative large-scale Pb-Zn deposit hosted in the late Ediacaran Dengying Formation dolostone in the SYGMP. The deposit is located in a triangular area bounded by the Jinsha River in the north, the Maozu reverse fault in the west and the Choushuijing fault in the southeast (Fig. 3a). Some folds are observed in the ore fields, such as the Ganshulin and Baika synclines and the Hongfadong and Changpo anticlines (Fig. 3a). The rocks in the Maozu ore fields are dominated by late Ediacaran carbonate rocks, Cambrian sediments (black shale, sandstone, and limestone) and Permian Emeishan basalts (Figs. 3a and 3b). The late Ediacaran Dengying Formation is the ore-hosting rock and is structurally controlled by the Maozu thrust fault-fold (Fig. 3a). The Permian Emeishan basalts are widely distributed in the western Maozu thrust fault (Fig. 3).

The ore bodies of the Maozu deposit are strictly controlled by stratigraphy (late Ediacaran Dengying Formation) and lithology (dolostone) and can be divided from shallow to deep into three types: upper layer (UL), vein layer (VL), and lower layer (LL) ore bodies. The VL connects the LL and UL (Fig. 3b), and these layers are characterized as follows. (1) The UL occurs in fine to coarse-crystalline stratiform dolomite that is below the phosphorus-bearing layer (Fig. 4a). The thickness is 15–30 m; predominant minerals are sphalerite, fluorite, and dolomite (Figs. 4a–4d), and minor amounts of tetrahedrite (Fig. 4d). (2) The VL ores occur in veinlets within the tectonic fractures (Fig. 4e) formed by ore-bearing hydrothermal fluids filling the cracks on both sides of the syngenetic fault (Gao et al. 2011; Liu et al. 2013). Pb-Zn ores are surrounded by breccias (Fig. 4f), in which the volume of galena in sulfide ore is relatively higher than that of the other two ore body types (He et al. 2006; Liu

FIGURE 1. Regional tectonic sketch map of southern China and the location of the Sichuan-Yunnan-Guizhou Pb-Zn metallogenic province (SYGMP) (modified from Huang et al. 2004; Zhou et al. 2018). (Color online.)



2009; Figs. 4g–4h), with fluorite, quartz, and calcite as the main gangue minerals. The VL is probably a secondary hydrothermal channel for ore-forming fluids (Gao et al. 2011; Liu et al. 2013). (3) The LL occurs in stratoid shape within siliceous dolostone. The ore body thickness varies from 50 to 120 m; the minerals are predominantly sphalerite and quartz (Figs. 4i–4l), and minor bitumen occurs around the sulfides (Fig. 4l).

The primary sulfide ores are predominantly made of sphalerite and galena, with minor pyrite and tetrahedrite. Gangue minerals consist of dolomite, calcite, fluorite, quartz, and bitumen. Ore textures and structures separately include the following: granular, porphyritic, and metasomatic (Figs. 4c, 4d, and 4k); massive, banded (Fig. 4i); and disseminated and veined (Fig. 4e). Wall rock alterations are principally dolomitization and calcification, which are closely associated with Pb-Zn mineralization.

Based on macro- to microscale geological observations, the paragenesis in the Maozu deposit has been identified. Fine pyrite (Py1) in sphalerite precipitated first (Figs. 4k and 4l), and the

particles of the fine pyrites are small due to replacement by later sphalerite or other sulfides. Under a microscope, the sphalerite is cross-cut by later galena veins (Figs. 4c and 4k), which also wraps around the coarse pyrite (Py2, Fig. 4k), i.e., the coarse pyrite and galena were formed simultaneously. The edges of the galena are, in some cases, replaced by later tetrahedrite (Fig. 4d and 4k). Fluorite is frequently cut by sphalerite and galena veins (Fig. 4g). The Pb-Zn ores are, in some cases, cut by calcite veins (Fig. 4b), which may indicate that the calcite (and dolomite) is the last mineral to form in the deposit. Based on the macro- to micro-scale geological observations, the mineralization stages in the Maozu deposit were divided into diagenetic, hydrothermal, and supergene stages (Fig. 5), and the simplified mineralization sequence is as follows:

Fine pyrite (Py1) → fluorite (Flu) → sphalerite (Sp) → galena (Gn) + coarse pyrite (Py2) → tetrahedrite (Tet) → quartz (Q) → calcite (Cal) + dolomite (Dol).

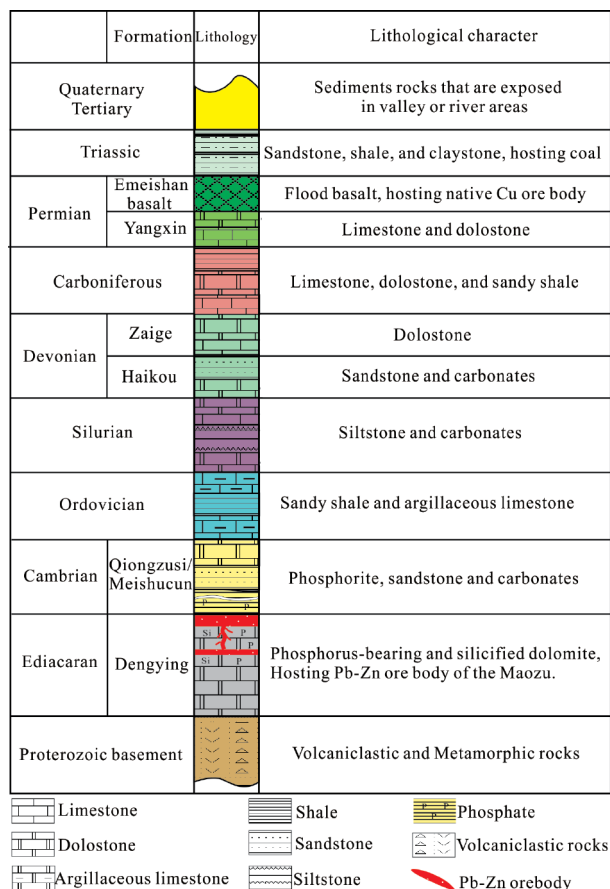


FIGURE 2. Generalized stratigraphic column of the Maozu Pb-Zn deposit (modified from Zhou et al. 2018). (Color online.)

ANALYTICAL METHODS

The sulfide samples were collected from all three types of ore bodies in the Maozu mine area, including six samples from the upper layer, four samples from the vein layer, and three samples from the lower layer. The details are listed in Table 1, and the sample locations are shown in Figure 3b. All samples were prepared as one-inch polished blocks.

LA-ICP-MS spot and mapping analyses of trace elements in sphalerite and galena were performed using the Agilent 7700x Quadrupole ICPMS instrument at CODES (University of Tasmania, Hobart, Australia) coupled with a high-performance RESOLUTION 193 nm ArF ATL excimer laser ablation system equipped with Geostar software. The diameter of the analytical spot was 30 μm . Trace-element analyses of the sphalerite (9 samples, 72 spots) and galena (4 samples, 26 spots) from the three ore bodies (UL, VL, and LL) were completed, and an average of 8 spots were analyzed for each sample. Each analysis was performed in the time-resolved mode, which involves sequential peak hopping through the mass spectrum. The laser system was operated at a consistent 5 Hz pulse rate, and the laser energy was typically 2.7 J/cm², with a dwell ratio of 3.0 $\mu\text{m}^2/\text{s}$. The masses of the following elements were measured: ⁵⁵Mn, ⁵⁷Fe, ⁵⁹Co, ⁶⁰Ni, ⁶⁵Cu, ⁶⁶Zn, ⁷²Ge, ⁷⁵As, ⁷⁷Se, ¹⁰⁷Ag, ¹¹¹Cd, ¹¹⁵In, ¹¹⁸Sn, ¹²¹Sb, ¹²⁵Te, ²⁰⁸Tl, ²⁰⁸Pb, and ²⁰⁹Bi. The analysis time for each sample was 90 s, including 30 s background with laser off and 60 s analysis with laser on. Acquisition time for all masses was set to 0.02 s, with a total sweep time of ~0.6 s. Calibration was performed using STDGL2b-2 (an in-house standard), which is suitable for quantitative analyses in different sulfide matrixes (Danyushevsky et al. 2003, 2011). For more details about the analytical process, please refer to Cook et al. (2009) and Ye et al. (2011).

Each measured values of sphalerite samples were adjusted by the following correction factors (Danyushevsky et al. 2011): Mn 1.46, Fe 1.49, Co 1.51, Ni 1.59, Cu 1.53, As 1.36, Se 1.85, Ag 1.40, Cd 1.50, In 1.45, Sn 1.60, Sb 1.17, Te 1.00, Tl 2.17, Pb 1.37, and Bi 1.33. These correction factors have been established by

analyzing sphalerite secondary standards using STDGL2b-2 and reflect the significant elemental fractionation between Zn and the other elements during ablation. The correction factor error is <5% (Cook et al. 2009). Whereas, the measured value of galena did not require correction.

The raw analytical data for each spot analysis were plotted as a line graph, and the integration times for background and sample signal were selected. The counts were then corrected for instrument drift (standards were run every 1½ to 2 h) and converted to concentration values using known values of Zn in the analyzed sphalerite as an internal standard. Data reduction was undertaken using Zn (640 600 ppm) as the internal standard for sphalerite and Pb (866 000 ppm) for galena.

RESULTS

The sphalerite (9 samples, 72 spots) and galena (4 samples, 26 spots) from three ore bodies (UL, VL, and LL) of the Maozu Pb-Zn deposits are summarized in Table 1, and the data include the mean, median, median absolute deviation (MAD), minima, and maxima for each selected sample. The ranges for each selected element in absolute concentrations are shown in Figure 6 (sphalerite) and Figure 7 (galena). Representative time-resolved profiles of the elements are shown in Figure 8. Complete LA-ICP-MS data sets can be found in electronic Appendix A (Supplemental Material¹).

During the analysis, the areas that are free of obvious inclusions or other features in the sulfides were chosen for the measurement. Flat and irregular (inconsistent with Zn and S profiles) acquisition profiles in the time-resolved depth acquisition profiles likely represent elements distributed as solid solutions and microscale inclusions, respectively. Inclusions were excluded during the data reduction.

Trace elements in sphalerite

Fe. The *iron* concentrations in the sphalerite of the Maozu deposit range from 698 to 20 570 ppm (median 6273 ppm, $n = 72$), which is the highest trace-element content in sphalerite and slightly lower than the *iron* content of the MVT deposit (Cook et al. 2009; Ye et al. 2011, 2016; Yuan et al. 2018) (Fig. 6). The Fe counts in the time-resolved depth acquisition profiles are flat and smooth (Figs. 8a–8c). The Fe concentrations of the sphalerite in the VL are the most enriched (Figs. 6 and 9c), and the Fe content changes in the order LL \rightarrow VL \rightarrow UL, with values of 1555–8156 ppm (median 2257 ppm, $n = 16$) \rightarrow 4386–20 570 ppm (median 9527 ppm, $n = 16$) \rightarrow 698–14 752 ppm (median 9257 ppm, $n = 40$), respectively.

Cd. *Cadmium* has the second-highest measured values in sphalerite with respect to any other element analyzed in this study. Its concentration ranges from 2237–4685 ppm (median 3465 ppm, $n = 72$), which is much higher than the content of by-products extracted from sphalerite (100–900 ppm) and consistent with the Cd content of MVT (Cook et al. 2009; Ye et al. 2011, 2016; Yuan et al. 2018). Cadmium was uniformly distributed in the mapping image (Fig. 10) and appeared as a smooth acquisition profile (Figs. 8a–8c). *Cadmium* is negatively correlated with Fe and Mn (Figs. 9a–9b). Moreover, the median contents of Cd tend to decrease from the LL to VL to UL at 3945 ppm ($n = 16$) \rightarrow 3678 ppm ($n = 16$) \rightarrow 3162 ppm ($n = 40$), respectively.

Cu. The *copper* concentrations are not constant and vary from 9.23 to 2752 ppm, with a median of 334 ppm ($n = 72$). The contents of Cu in sphalerite are similar to those in MVT (Cook et al. 2009; Ye et al. 2011, 2016; Yuan et al. 2018) (Fig. 6). Although Cu is unevenly distributed in the mapping images and has overlapping enrichment areas with Ge, Sb, and Ag (Fig. 10), the acquisition profiles of Cu, Ge, Sb, and Ag are parallel to the Zn and S

acquisition profile (Fig. 8d). Furthermore, the distribution in the (Cu + Sb) vs. (Ag + Ge) plot (Fig. 9k) exhibits a strong positive correlation ($r = 0.80$).

Sn. The *tin* concentrations in the Maozu deposit are abnormally enriched compared with those in the typical MVT deposit (Cook et al. 2009) and reach the values observed in skarn and massive sulfide deposits (Cook et al. 2009; Ye et al. 2011) (Fig. 6), which vary from 0.05 to 2192 ppm (median 1.52 ppm, $n = 71$). The Sn concentration range is relatively wide, but the majority of Sn is low and only partially enriched. Sn is positively correlated with In ($r = 0.82$, Figs. 9j and 10). The acquisition profiles of Sn are analogous with those of In and parallel to the Zn and S acquisition profiles (Fig. 8c). Sn is most abundant in the VL, and the Sn contents in the LL, VL, and UL vary from 0.06–14.5 ppm (median 0.25 ppm, $n = 16$), 0.1–2192 ppm (median 54.8 ppm, $n = 16$), and 0.05–179 ppm (median 1.67 ppm, $n = 39$), respectively.

In. The *indium* concentrations in sphalerite of different deposit types vary, as shown in Figure 6. The skarn and massive sulfide

deposits (Cook et al. 2009; Ye et al. 2011) contain the highest concentration of In, whereas low In contents were observed in the MVT (Fig. 6; Cook et al. 2009; Ye et al. 2011, 2016; Yuan et al. 2018). The In concentration in Maozu extends from 0.001 to 1191 ppm, with a median of 2.84 ppm ($n = 66$). A remarkable feature is that the maximum concentration of In in the Maozu deposit has reached the levels observed in typical skarn and massive sulfide deposits (Cook et al. 2009; Ye et al. 2011), which are much higher than the In levels of the MVT. Additionally, In and Sn show the same element enrichment areas (Fig. 10). The acquisition profile of In is smooth and parallel to Sn, Zn, and S on the time-resolved depth profiles (Fig. 8c). Similar to Sn, In is most enriched in the VL (Figs. 6 and 9j); the variation of In is in the order LL → VL → UL, with values of 0.01–464 ppm (median 0.94 ppm, $n = 13$) → 0.001–1191 ppm (median 35.7 ppm, $n = 15$) → 0.01–397 ppm (median 1.40 ppm, $n = 38$), respectively.

Sb. The *antimony* content is relatively low in the skarn and massive sulfide deposits, but those in typical MVT deposits are

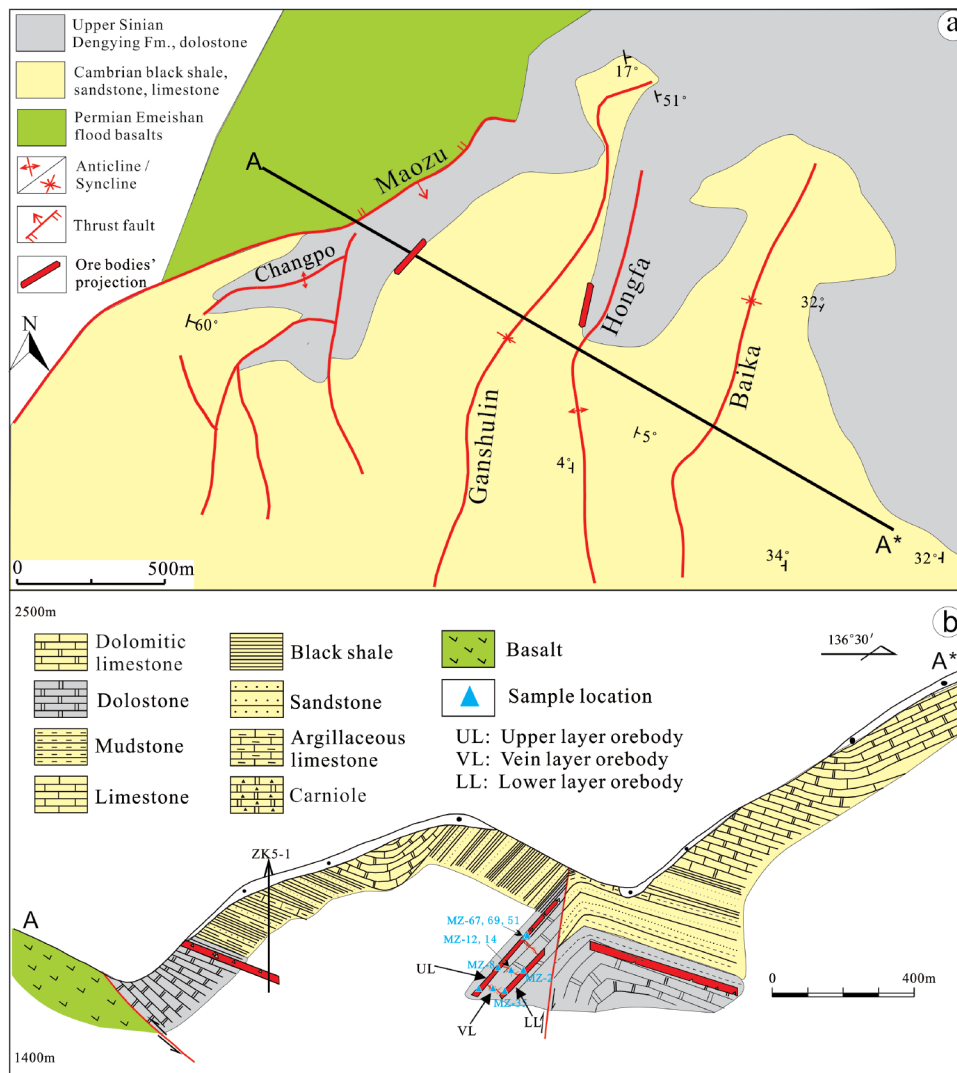


FIGURE 3. (a) Geological map of the Maozu Pb-Zn deposit (modified after Liu 2009). (b) Representative cross section A–A* through the deposit. (Color online.)

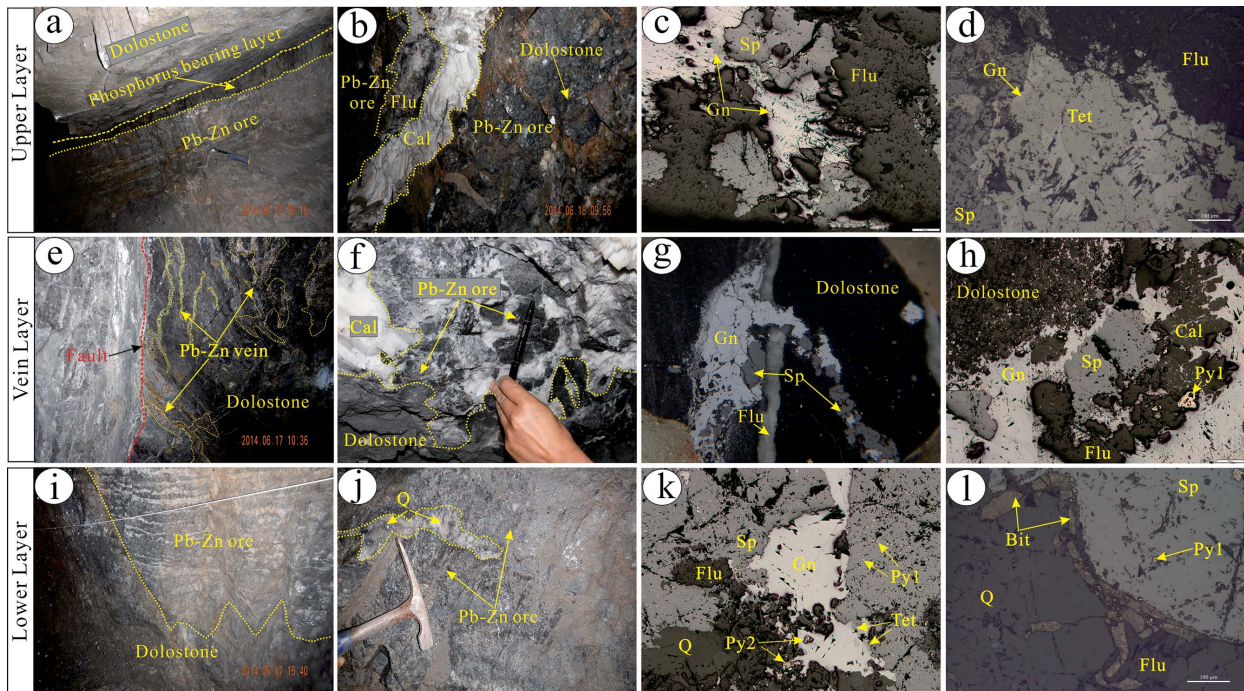


FIGURE 4. Outcrop photographs coupled with photomicrographs of thin sections from lower layer (LL), vein layer (VL), and upper layer (UL)—three ore bodies in the Maozu deposit. (a) UL occurs as stratiform in dolostone below the phosphorus-bearing layer. (b) Gangue minerals in the UL are dominated by fluorite and dolomite. (c) Sphalerite is cross-cut by a later galena vein. (d) Galena edges are replaced by later tetrahedrite. (e) VL ore bodies occur as veinlets in the tectonic fractures. (f) Pb-Zn ores coexist with calcite. (g) Fluorite is cut by sphalerite and galena veins. (h) Galena is wrapped with coarse pyrite (Py2). (i) LL occurs in siliceous dolomite as in stratoid form. (j) Quartz is the dominant gangue mineral in the LL. (k) Fine pyrite (Py1) in sphalerite formed earlier than sphalerite. (l) Minor bitumen occurs around the sulfides. Abbreviations: Sp = sphalerite; Gn = galena; Py = pyrite; Tet = tetrahedrite; Flu = fluorite; Q = quartz; Cal = calcite; Dol = dolomite and Bit = bitumen; UL = upper layer; VL = vein layer; and LL = lower layer. (Color online.)

relatively high (Cook et al. 2009; Ye et al. 2011) (Fig. 6). The concentration of Sb in the sphalerite of the Maozu deposit is 0.35–835 ppm (median 36.3 ppm, $n = 71$), and it presents a wide variation range and a nonuniform distribution. As previously described, Sb has the same enrichment characteristics as Cu, Ge, and Ag (Fig. 10), and these elements have a strong positive correlation ($r = 0.83$, Figs. 9h, 9k–9m). The profile of Sb is smooth and is parallel to those of Cu, Ge, Ag, Zn, and S (Fig. 8d).

Pb. The lead content shows an uneven enrichment in the mapping image (Fig. 10), and the concentrations are within the range of 0.62–399 ppm (median 8.22 ppm, $n = 72$). The ragged and irregular profiles (Fig. 8b) imply that Pb is present as micro-inclusions in sphalerite rather than as a solid solution. Pb and As have similar profiles.

Ge. The germanium content ranges widely from 0.30–342 ppm (median 36.9 ppm, $n = 72$), and the Ge concentrations within sphalerite from the Maozu deposit are consistent with those in the MVT (Cook et al. 2009; Ye et al. 2011, 2016; Yuan et al. 2018) while low levels were observed in typical skarn (Cook et al. 2009; Ye et al. 2011) and massive sulfide deposits (Cook et al. 2009 and references therein; Ye et al. 2011). The spectrum of Ge is smooth (Figs. 8b and 8d). Ge shares similar enrichment areas with Cu, Sb, and Ag in the mapping images and is positively correlated with these elements (Figs. 9e, 9h, and 9k).

As. The arsenic content in the sphalerite of Maozu varies

from 0.75 to 275 ppm (median 9.36 ppm, $n = 58$), which is more enriched than that in the skarn (Cook et al. 2009; Ye et al. 2011) and massive sulfide deposits (Cook et al. 2009 and references therein; Ye et al. 2011) but similar to the concentration in the MVT deposits (Fig. 6). Most of As show smooth LA-ICP-MS down-hole spectral profiles, but several anomalous LA-ICP-MS time-resolved signal spectra (Fig. 8d) could be observed, as is consistent with that of Pb. In the mapping images, arsenic also

MINERAL	Diagenetic stage	Hydrothermal stage		Supergene stage
		Early-ore stage	Late-ore stage	
Fine pyrite (Py1)		Less	More	
Fluorite		Less	More	
Sphalerite		Less	More	
Galena		Less	More	
Coarse pyrite (Py2)		Less	More	
Tetrahedrite		Less	More	
Quartz		Less	More	
Calcite		Less	More	
Dolomite		Less	More	
Smithsonite		Less	More	
Cerussite		Less	More	

— Less — More

FIGURE 5. Mineral paragenesis in the Maozu Pb-Zn deposit.

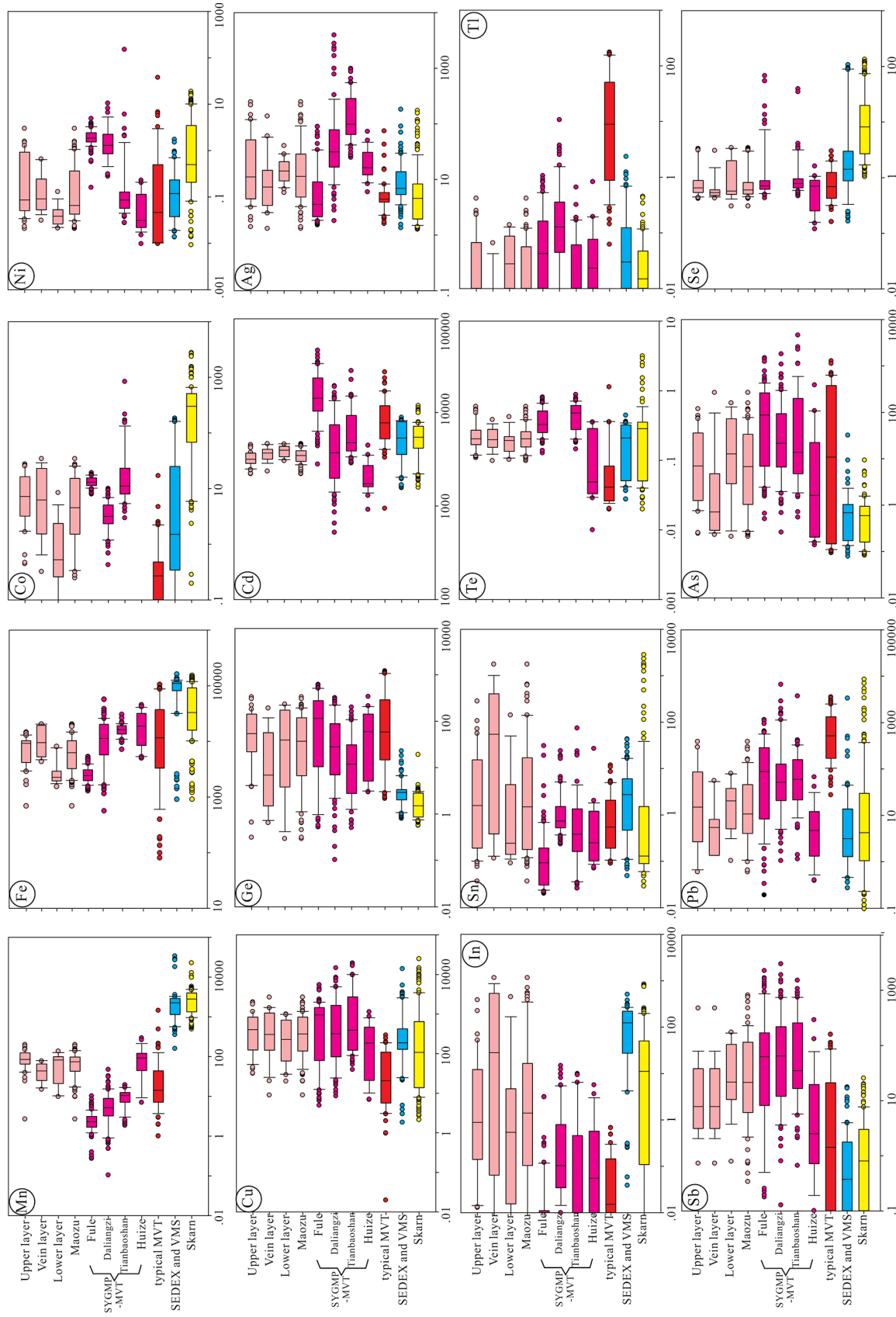


FIGURE 6. Trace element concentrations (LA-ICP-MS) in sphalerite from the Maozu Pb-Zn deposit and trace element concentrations in different genesis deposits [the data on the skarn, SEDEX, VMS, MVT, and Huize are from Ye et al. (2011); data on Tianbaoshan are from Ye et al. (2016); data on Daliangzi are from Yuan et al. (2018); and data on Fule are from Li (2016)]. (Color online.)

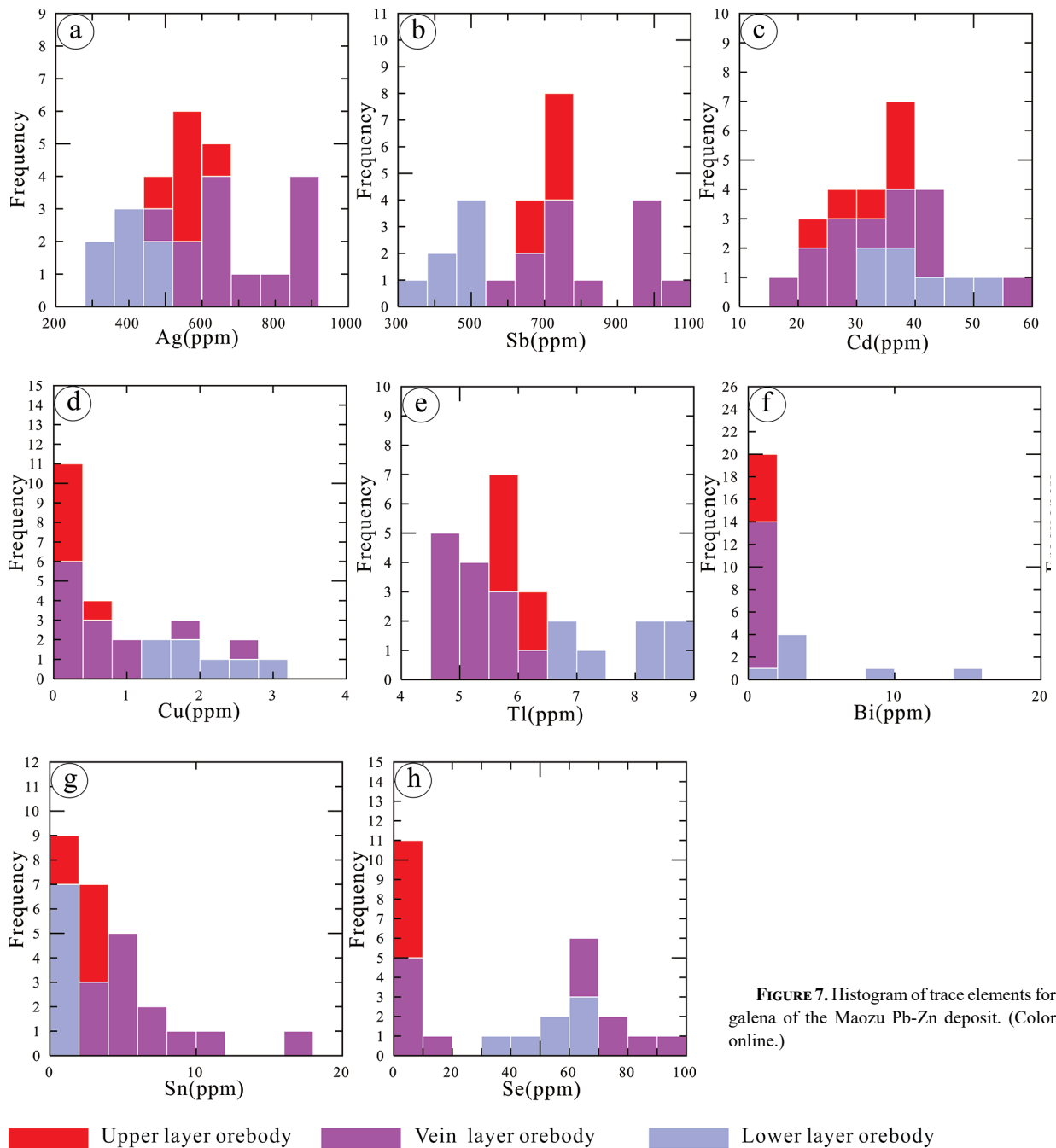


FIGURE 7. Histogram of trace elements for galena of the Maozu Pb-Zn deposit. (Color online.)

shows a relatively concordant distribution with Pb.

Ag. The *silver* concentrations range from 1.34–254 ppm (median 12.5 ppm, $n = 72$), and a certain amount of Ag was found in all samples. The Ag contents in the deposits with different genesis types are similar (Fig. 6). Although Ag is unevenly distributed in the mapping images (Fig. 10), the Ag enrichment areas are consistent with those of Cu, Ge, and Sb (Fig. 10). In addition, all spot analyses show that Ag shows a positive correlation with Cu ($r = 0.59$, Fig. 9f), Ge ($r = 0.48$, Fig. 9g), and Sb ($r = 0.76$), respectively.

Mn. The *manganese* content presents a relatively narrow distribution range (Table 1; Fig. 6), with concentrations from

2.78–206 ppm (median 74.5 ppm, $n = 72$). The Mn contents gradually increased from the center to the edge of the sphalerite particles in the mapping image (Fig. 10). The concentration of Mn is generally consistent with that of the MVT deposits but significantly lower than that of the massive sulfide and skarn deposits.

Co. *Cobalt* concentration varies 3 orders of magnitude, ranging from 0.04 to 35.1 ppm (median 4.59 ppm, $n = 71$), which is slightly higher than that of the MVT deposits (Fig. 6). A positive correlation between Co and Ni was observed in Figure 9d, and there is a correlation between the distributions of Co and

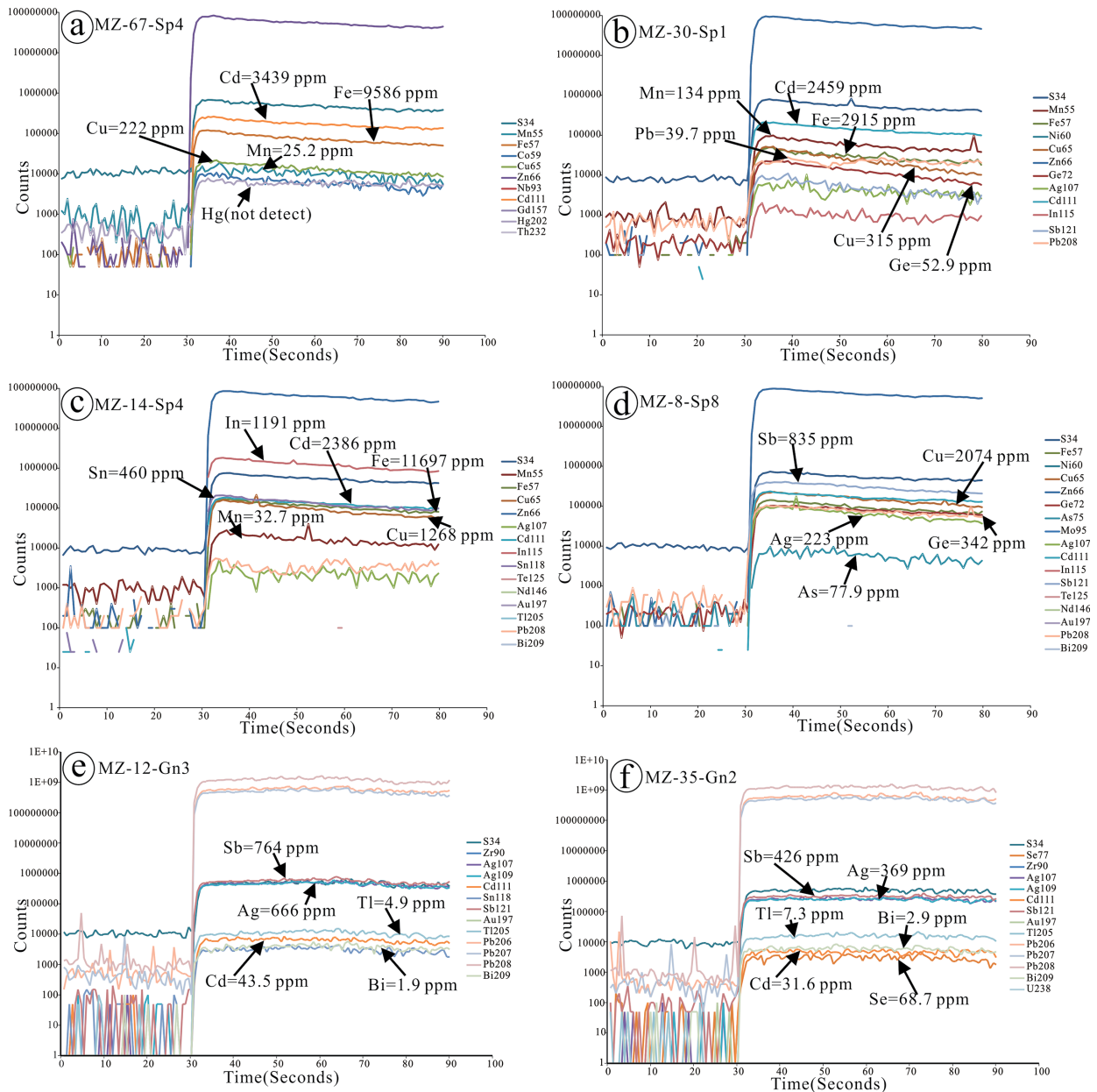


FIGURE 8. Representative time-resolved depth acquisition profiles for sphalerite (a–d) and galena (e–f) analyzed by LA-ICP-MS. (Color online.)

Fe (Fig. 10). From the LL to UL, Co shows a trend of gradual enrichment (Fig. 9d). In the profiles, Co presents a flat and smooth acquisition profile that is nearly parallel to that of Fe.

Ni. The nickel concentrations are relatively low, with most below the detection limit, and the maximum is only 3.08 ppm and medians are lower than the concentrations in the massive sulfide and skarn-type sphalerites (Fig. 6). Due to the low contents, the Ni acquisition profiles cannot be shown in the LA-ICP-MS profiles. However, Ni is evenly distributed in the mapping image of sphalerite (Fig. 10). Co and Ni have a strong positive correlation (Fig. 9d).

Se. The selenium concentration in sphalerite from the Maozu deposit is mostly lower than the detection limit, and the maximum content is only 3.52 ppm, which is analogous to the concentrations

in the MVT and lower than that in the skarn deposits (Fig. 6).

In addition, the concentrations of other elements, such as Te, Tl, and Bi, from the Maozu deposit have been detected at a few spots with the contents mostly below the detection limits (Supplemental Material¹ Appendix A). Although the Hg acquisition profile is obvious in the measured samples (Fig. 9a), an accurate Hg value cannot be obtained because there is no available sample standard.

Trace elements in galena

Sb. Antimony is the most enriched element in galena of the Maozu deposit (Fig. 7b), ranging from 342 to 1033 ppm (median 724 ppm, $n = 26$). Sb and Ag are positively correlated (Fig. 9n) and both show smooth LA-ICP-MS acquisition profiles (Figs.

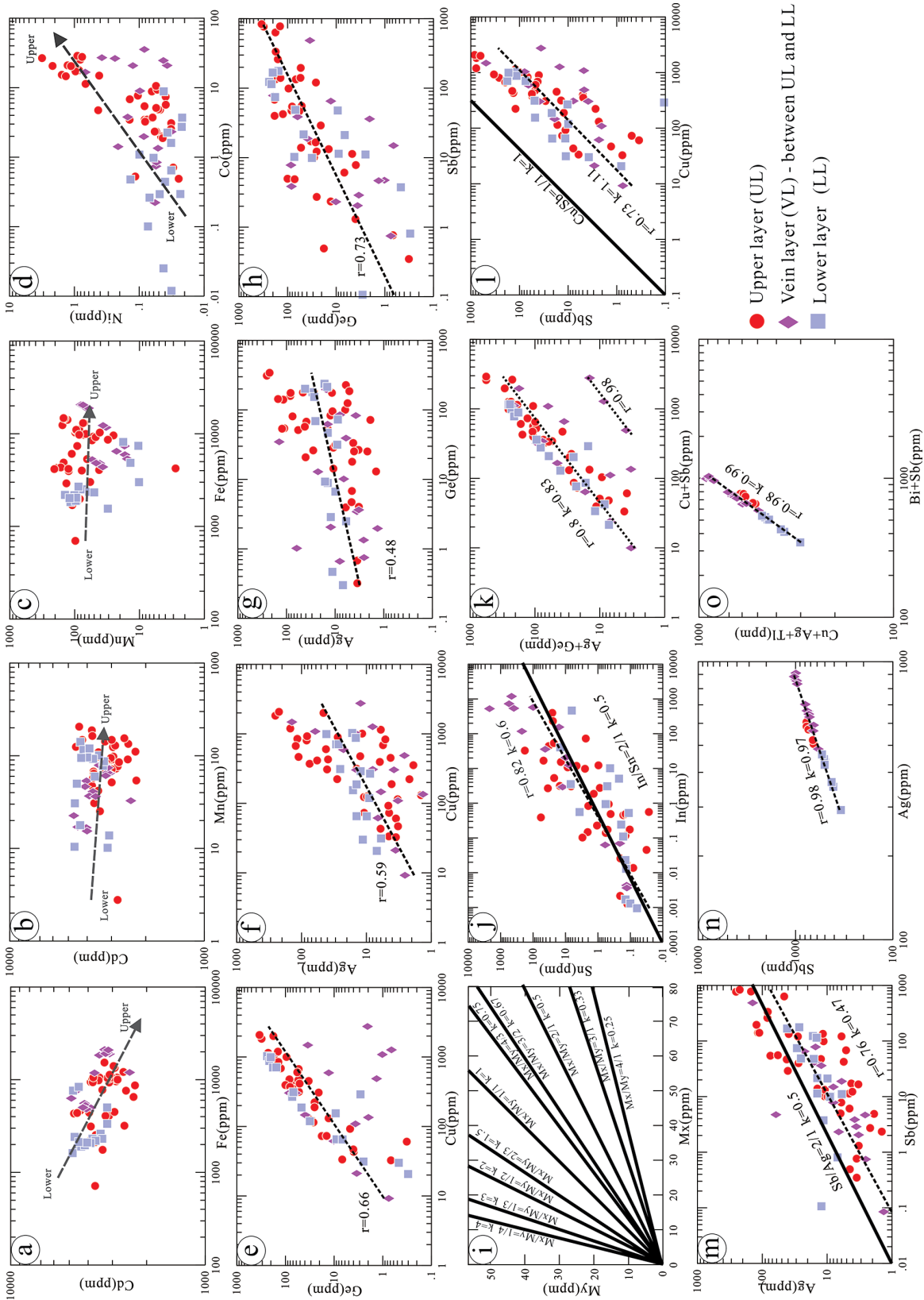


FIGURE 9. Correlation plots of sphalerite: (a) Fe vs. Cd, (b) Mn vs. Cd, (c) Fe vs. Mn, (d) Co vs. Ni, (e) Cu vs. Ag, (f) Cu vs. Ge, (g) Ge vs. Ag, (h) Sb vs. Ge, (i) Mx vs. My, (j) In vs. Sn, (k) (Cu + Sb) vs. (Ag + Ge), (l) Cu vs. Sb, (m) Sb vs. Ag, Galena of (n) Ag vs. Sb, and (o) (Bi + Sb) vs. (Cu + Ag + Tl). Note: r = correlation coefficient; k = slope; dashed lines = regression lines; solid lines = lines with different WRs. (Color online.)

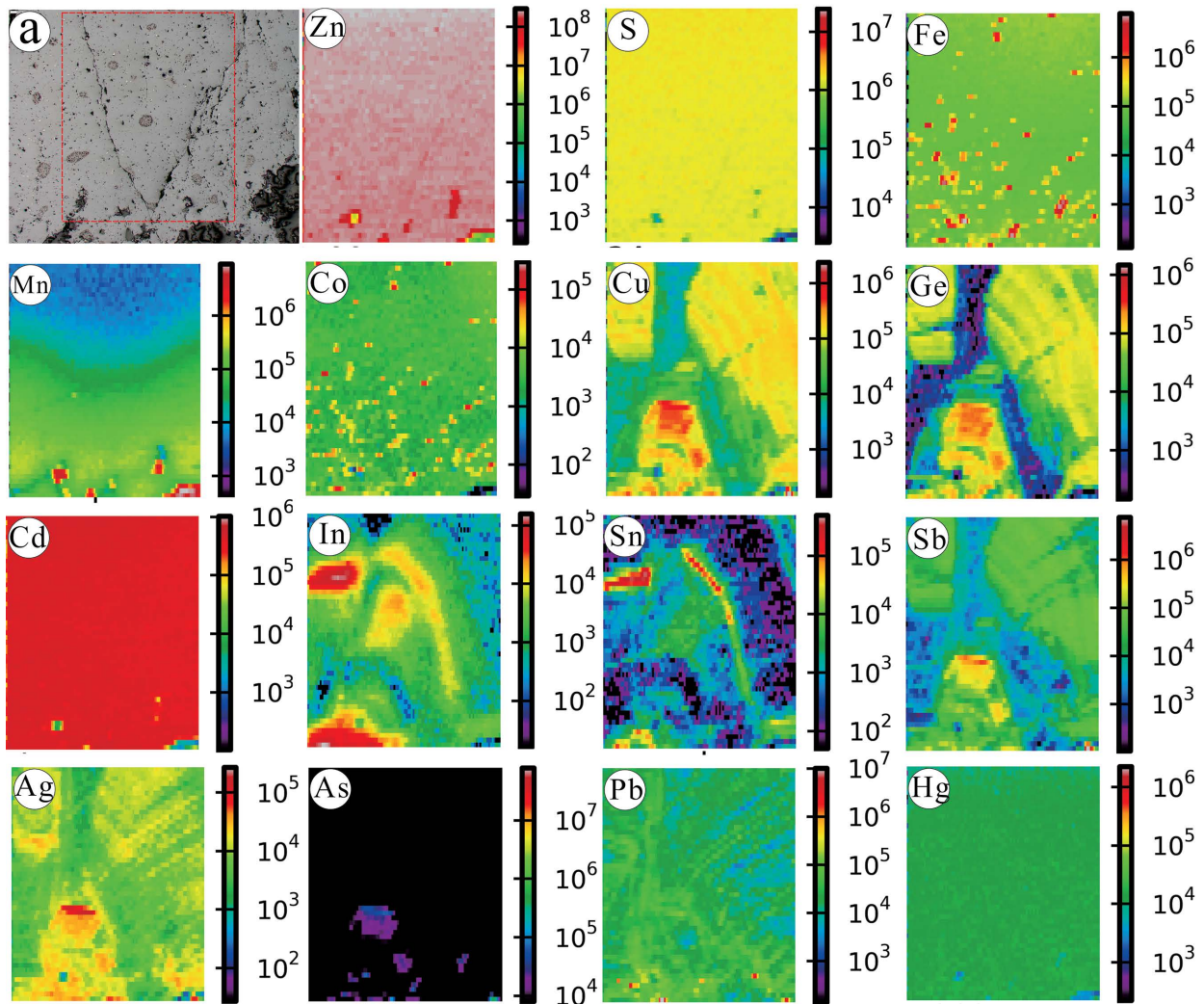


FIGURE 10. Mapping images of sphalerite in the Maozu Pb-Zn deposit. The rectangle in the first image (a) is the scanning area of sphalerite. (Color online.)

8e–8f). Sb contents gradually increase from the LL (498 ppm, $n = 7$) to the UL (740 ppm, $n = 6$), with the highest concentration in the VL ore body (764 ppm, $n = 13$).

Ag. Silver is widely distributed in galena of the Maozu deposit (Fig. 7a), ranging from 293–910 ppm (median 582 ppm, $n = 26$). There is a very strong positive correlation between Ag and Sb ($r = 0.98$, $n = 26$; Fig. 9n). In the time-resolved depth acquisition profiles, Ag and Sb appear as flat acquisition profiles that are parallel to the Pb and S (Figs. 8e–8f). From the LL (median 426 ppm, $n = 7$) to the UL (median 575 ppm, $n = 6$), Ag gradually increases, and the content of Ag in the VL (median 666 ppm, $n = 13$) is the highest (Fig. 7a).

Se. Selenium is relatively enriched in the galena of the Maozu deposit from 0.44–96.4 ppm (median 56.6 ppm, $n = 22$). Although Se is widely distributed (Fig. 7h), Se appears in a flat acquisition profile in the time-resolved depth acquisition profiles (Fig. 8f).

Cd. Cadmium is relatively enriched and concentrated in the galena from the Maozu deposit and presents a normal distribution (Fig. 7c) from 19.7–56.7 ppm (median 36.1 ppm, $n = 26$). The

Cd acquisition profile is smooth, flat, and is parallel to those of Pb and S. The Cd in galena from the three ore bodies shows no obvious differences.

Sn. Tin content in galena is relatively low, with most concentrations <10 ppm, and the variation range is 0.61–16.6 ppm (median 2.74 ppm, $n = 26$). From the LL to VL to UL, the median contents change from 0.76 ppm ($n = 7$) to 5.29 ppm ($n = 13$) to 2.33 ppm ($n = 6$), respectively, and the highest Sn concentration occurs in the VL.

Bi. Bismuth content in galena is mostly <10 ppm (Fig. 7f), and it ranges from 0.01–14.2 ppm (median 0.48 ppm, $n = 26$). The Bi acquisition profile is smooth and flat and parallel to the Pb and S acquisition profiles (Fig. 8f). The correlation between Bi and Sb is strong (Fig. 9o).

Tl. Thallium is the most concentrated trace element in the galena of the LL (Fig. 7e), and the total content range is 4.73–8.59 ppm (median 5.76 ppm, $n = 26$). The acquisition profile of Tl is smooth and flat (Figs. 8e–8f). From LL \rightarrow VL \rightarrow UL, the median content changes from 8.15 ppm ($n = 7$) \rightarrow 5.17 ppm ($n = 13$) \rightarrow

5.84 ppm ($n = 6$), respectively.

Cu. *Copper* is present in relatively low concentrations except in the LL, where its concentration is relatively high (Fig. 7d). The Cu concentrations in the VL and UL are all <1 ppm, and the total distribution range is 0.15–3.04 ppm (median 0.67 ppm, $n = 24$). The correlation between Cu and Tl is strong (Fig. 9o).

In addition, other elements in the galena from the Maozu deposit, such as Fe, Mn, and As, are generally below the minimum detection limit.

DISCUSSION

Occurrence and substitution mechanisms of trace elements

LA-ICP-MS analysis can provide significant information for the occurrence of a particular element. Micro-inclusions are commonly noted in the LA-ICP-MS acquisition profiles (peak) if they are sufficiently large (e.g., Cook et al. 2009; Ye et al. 2011, 2016; George et al. 2015), whereas lattice-bound trace elements and nanoparticles would present flat features in the signal spectra and thus are hard to distinguish (e.g., Gregory et al. 2014, 2015). In those cases, trace-element mapped images may provide additional constraints on the occurrence of the elements in hosted minerals. But the hypothesis that these elements may occur as nanoparticles could not be ruled out.

The occurrence of trace elements in sphalerite. Although trace elements of Mn, Cd, Fe, and Co show high variations (Table 1; Fig. 6), these trace elements occur as smooth and flat and follow changes of Zn and S in the LA-ICP-MS acquisition profiles (Fig. 8a). Moreover, these elements are uniformly distributed in the trace-element mapping images (Fig. 10), suggesting that these elements likely mainly occur as solid solutions in sphalerite. Notably, in the mapping images (Fig. 10), from the center to the edge of the sphalerite particles, Mn contents gradually increase, probably because of the later formation of hydrothermal dolomite that contains a certain amount of Mn. Additionally, several spot-like concentration areas enriched Fe and Co are evenly distributed in the mapping images (Fig. 10), which may be attributed to the disseminated pyrite in the sphalerite (Figs. 4k and 10a) and indicates that the Co enrichment is related to the Fe distribution.

The concentrations of elements In, Sn, Cu, Ge, Sb, and Ag vary widely (Fig. 6), and these trace elements are unevenly distributed in the mapping images. However, the element acquisition profiles are flat and smooth, which is consistent with the Zn and S acquisition profiles (Figs. 8c and 8d), implying that these elements did not exist as micro-inclusions. In, Sn, Cu, Ge, Sb, and Ag have overlapping element enrichment areas in the mapping images (Fig. 10), suggesting that these elements may enter into the sphalerite crystal structure by coupled substitution.

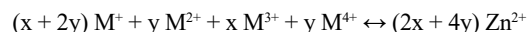
The sphalerite contains measurable concentrations of Pb and As, which typically vary greatly (Fig. 6) and are unevenly distributed in the mapped images (Fig. 10). Several acquisition profiles appear as ragged and irregular in the time-resolved profiles and show a coordination change with the profile of Pb (Fig. 8d), suggesting partly Pb and As exist in sphalerite as micro-inclusions.

The concentrations of Bi, Tl, Ni, Se, and other trace elements are extremely low (<5 ppm), and the acquisition profiles of these elements could not be reflected in the LA-ICP-MS profiles.

The occurrence of trace elements in galena. Although the Ag and Sb concentrations vary widely, their spectral profiles present

smooth and flat features and are parallel with the Pb and S in the time-resolved profiles (Figs. 8e–8f), which may indicate that Ag and Sb likely enter into the galena crystal structure. Meanwhile, Cd, Se Bi, and Tl appear as smooth and flat profiles, which is consistent with the changes in the Pb and S (Figs. 8e and 8f), revealing that these elements may also occur as solid solutions in galena.

Substitution mechanisms. Many studies have demonstrated that the bivalent cations (e.g., Cd^{2+} , Fe^{2+} , Mn^{2+} , Co^{2+}) are easily incorporated into sphalerite via simple substitution of Zn^{2+} , due to the similar ion radii (Johan 1988; Cook et al. 2009). Tri- and tetravalent elements (e.g., Ge^{4+} , Sb^{4+} , In^{3+}) are thought to enter sphalerite via coupling with monovalent elements (Cu^+ , Ag^+) or through the creation of vacancies (e.g., Bernstein 1985, 1986; Cook et al. 2009, 2012; Ye et al. 2011; Belissont et al. 2014; Wei et al. 2019). Johan (1988) proposed a general coupled substitution mechanism for trivalent and tetravalent elements in sphalerite as follows:



where $\text{M}^+ = \text{Ag}$, Cu ; $\text{M}^{2+} = \text{Cu}$, Fe , Cd , Hg , Zn ; $\text{M}^{3+} = \text{In}$, Ga , Fe , Tl ; $\text{M}^{4+} = \text{Ge}$, Sn , Mo , W ; and x and y are atomic proportions of M^{3+} and M^{4+} , respectively. However, the substitution mechanisms for these elements are still debated. For example, some authors proposed the intake of Ge^{2+} in sphalerite via direct substitutions ($\text{Zn}^{2+} \leftrightarrow \text{Ge}^{2+}$) (e.g., Cook et al. 2009; Ye et al. 2011). In contrast, Cook et al. (2015) postulated that Ge enters the sphalerite structure through the creation of vacancies such as $2\text{Zn}^{2+} \leftrightarrow \text{Ge}^{4+} + \square$. Wei et al. (2019) considered that Cu and Ge show a coupled substitution of Zn ($3\text{Zn}^{2+} \leftrightarrow 2\text{Cu}^+ + \text{Ge}^{4+}$) due to the correlation between Ge and Cu with a trend to parallel to the molar ratio $(\text{Cu}/\text{Ge})_{\text{mol}} = 2$.

The atomic ratio (AR) was an effective method to understand the substitution mechanisms of trace elements in sphalerite (e.g., Johan 1988; Belissont et al. 2014; Wei et al. 2019). Therefore, it was applied to determine the substitution of the tri- and tetravalent elements in sulfide from Maozu. Based on the results of Johan (1988), the slope (k) of different ARs is determined according to the weight ratio (WR) (Mx/My) of the elements to make a line (Fig. 9i) with different ARs (i.e., different slopes). Even in different coordinate systems, the slope (k) is constant due to the constant WR; therefore, the AR is also constant. The AR of each element in the substitution reaction can be determined according to the slope of the regression line in the correlation plot (Fig. 9i). The premise of the application of this plot (Fig. 9i) is that Mx and My have a good linear relationship, basically presenting a linear distribution (e.g., Figs. 9j–9o), and the contents of elements are concentrated and cannot be scattered (Figs. 9e–9h); otherwise, the calculated AR is not accurate.

As noted above, although In and Sn are not evenly distributed in sphalerite, these elements have similar element distribution features in the mapped images and show a good linear relationship in Figure 9j ($r = 0.82$, $n = 66$), indicating that these elements are coupled substitutions for Zn in sphalerite; a similar result has been reported by Belissont et al. (2014). Other than In and Sn, there may be the presence of vacancies (represented by \square) for other uncertain elements. According to the equation of Johan (1988), the possible substitution equation is $x\text{In}^{3+} + y\text{Sn}^{4+} + z\square \leftrightarrow (x + y + z) \text{Zn}^{2+}$.

As the plots are concentrated and linearly distributed in the In-Sn correlation plot, the regression line ($r = 0.82$, $k = 0.6$) is ap-

proximately parallel to $\text{In/Sn} = 2/1$ ($k = 0.5$) (Fig. 9j). The slope of the regression line is slightly higher than the slope of the line with an AR of 2/1, which is attributed to the existing vacancies (\square). The atomic ratio of In^{3+} and Sn^{4+} is 2/1; therefore, the most likely coupled substitution is $2\text{In}^{3+} + \text{Sn}^{4+} + 2\square \leftrightarrow 5\text{Zn}^{2+}$.

Cu, Ge, Ag, and Sb have consistent element distribution characteristics in the mapping images, and $(\text{Cu} + \text{Sb})$ vs. $(\text{Ag} + \text{Ge})$ ($r = 0.8$, $n = 72$, Fig. 9k) shows strongly positive correlations. Therefore, these characteristics reveal that the elements are incorporated into sphalerite by coupled substitution. In the correlation plots of Cu vs. Ge (Fig. 9e), Cu vs. Ag (Fig. 9f), Ge vs. Ag (Fig. 9g), and Sb vs. Ge (Fig. 9h), the corresponding plots are scattered or not linearly distributed; thus, the AR cannot be determined. Although the correlation coefficients of $(\text{Cu} + \text{Sb})$ vs. $(\text{Ag} + \text{Ge})$ reached 0.8 ($n = 69$) and 0.98 ($n = 3$), there are two groups of linear relations (Fig. 9k), which suggested that other metal atoms (vacancies) may participate in the substitution; therefore, the AR cannot be determined by these plots.

The plots of Cu vs. Sb ($r = 0.73$, $k = 1.11$, Fig. 9l) and Sb vs. Ag ($r = 0.76$, $k = 0.47$, Fig. 9m) are concentrated and linearly distributed, and their slopes are approximately parallel to those of the AR, at 1/1 ($k = 1$) and 2/1 ($k = 0.5$), respectively. The atomic ratio of Cu/Sb is 1/1 and that of Sb/Ag is 2/1. According to the equation of Johan (1988), Ge is tetravalent and Ag is monovalent. Belissont et al. (2014) reported Sb is trivalent and Cu is monovalent, in agreement with the results of AR. As noted above, other uncertain atoms (vacancies) may participate in the substitution, which may cause the coupled substitution of these elements (Cu, Ge, Ag, and Sb) to be slightly different from the equation of Johan (1988). Consequently, the possible coupled substitution is $4(\text{Cu}^{+} + \text{Sb}^{3+}) + (\text{Ge}^{4+} + 2\text{Ag}^{+}) + 2\square \leftrightarrow 13\text{Zn}^{2+}$.

Regarding galena, the contents of Ag and Sb vary greatly (Figs. 7a–7b). Conventionally, many researchers on galena have principally focused on elements with high concentrations, such as Ag, Sb, and Bi (Van Hook 1960; Jeppsson 1989; Lueth et al. 2000; Chutas et al. 2008; Renock and Becker 2011). *Thallium* is more readily incorporated into the crystal structure of galena with Bi, Ag, and Sb by coupled substitution due to the existence of Cu (George et al. 2015). Although all these elements have good linear relationships ($r = 0.98$, $n = 26$) in the correlation plots of Ag vs. Sb (Fig. 9n) and $(\text{Bi} + \text{Sb})$ vs. $(\text{Cu} + \text{Ag} + \text{Tl})$ (Fig. 9o), the coupled relationship of Ag and Sb is only considered because of the low contents of Bi, Cu, and Tl in galena from the Maozu deposit. The regression line slope of Ag vs. Sb ($k = 0.97$, Fig. 9n) is close to 1 (AR is 1/1), and thus $\text{Ag/Sb} = 1/1$. Additionally, previous studies generally treated Ag as monovalent and Sb as trivalent (Renock and Becker 2011; George et al. 2015; Ye et al. 2016). Hence, the coupled substitution between Ag, Sb, and Pb may be simplified as $\text{Ag}^{+} + \text{Sb}^{3+} \leftrightarrow 2\text{Pb}^{2+}$.

Mineralization temperature

Many studies have indicated that trace elements in sphalerite have a close connection with the temperature during sulfide precipitation; therefore, the contents of trace elements in sphalerite can indicate the temperature of mineral formation (Ofstedahl 1940; Möller 1987; Mladenova and Valchev 1998; Kelley et al. 2004; Frenzel et al. 2016). Conventionally, sphalerite enriched in Fe, Mn, In, Sn, and Te indicates sulfide formation under a high-temperature

condition, while sphalerite formed at low temperature is enriched in Cd, Ga, and Ge with a low In/Ge ratio (Ye et al. 2016). Sphalerite in the Maozu deposit is characterized by the enrichment of Cd and Ge and depletion of Fe, Mn, Co, Se, and Te. Fe content (698.1–20570 ppm) in sphalerite from the Maozu deposit is similar to the Fe content (0.6–4.2 wt%) in sphalerite formed at 100–200 °C according to Kelley et al. (2004). The compositions of the trace elements in sphalerite from the Maozu Pb-Zn deposit show enrichment of low-temperature elements, such as Cd and Ge, which are consistent with those in the typical MVT Pb-Zn deposits (Cook et al. 2009; Ye et al. 2011) (Fig. 6).

Cao et al. (2014) showed that the sphalerite formed at high temperature (200–355 °C) has a dark color and is rich in Fe (3.58–11.42%) and Mn (0.2–0.4%), whereas sphalerite formed at low temperature (110–180 °C) is lighter and relatively depleted in Fe (0.23–2.0%) and Mn (0.003–0.05%). The colors of the sphalerite in the Maozu Pb-Zn deposit are dominated by brown and yellow (Figs. 4a, 4e, and 4j). The contents of Fe and Mn are 0.07–2.1% and ~0.02%, respectively, which are similar to the contents of Fe and Mn in low-temperature sphalerite. These characteristics indicate that the mineralization temperature of the sphalerite in the Maozu Pb-Zn deposit is mainly medium to low temperature.

Frenzel et al. (2016) demonstrated that the trace-element concentrations (Ga, Ge, In, Fe, Mn, Ag, Co, and Cu) of sphalerite could be used to calculate the formation temperature. Because our experiment did not analyze the content of Ga, we use the Ga content (~20 ppm, Ye et al. 2011) from the Huize deposit (a typical Pb-Zn deposit in SYGMP that is similar in geological and geochemical features to the Maozu deposit) as a proxy according to the data from Frenzel et al. (2016). As a result, the formula (Frenzel et al. 2016) for calculating the ore-forming temperature of sphalerite was used, and the considered trace elements were Fe, Ge, In, and Mn from this study and Ga from Huize. The calculated ore-forming temperature of sphalerite in the Maozu deposit is 120.5–288.7 °C (average 179.3 °C), which is similar to a previous analysis of fluid inclusions in the Maozu deposit (140–280 °C, Yang et al. 2017), revealing that the ore-forming fluids of the deposit are medium-low temperature fluids.

In addition, the concentrations of In and Sn in the VL are the highest (Figs. 6 and 9j), and relatively more galena occurs in the VL than in the LL and UL (Fig. 4). These characteristics may indicate that the VL is the secondary channel for the migration of ore-forming fluids. The concentrations of Fe, In, and Sn in sphalerite and Ag and Sb in galena are the most enriched in the VL (Fig. 6). This finding may suggest that ore-forming fluid migration occurs from deep to shallow and that the VL connects the UL and LL by tectonic fracture zone and is the secondary migration channel of the ore-forming fluids.

Ore genetic type

The sulfide ore bodies of the Maozu deposit mainly occurs as stratiform and lentiform bodies, resulting in some researchers consider it as a sedimentary reworked type or SEDEX-type of deposit (e.g., Chen 2002; He et al. 2006). In fact, the ore-hosting rock is the late Ediacaran Dengying Formation dolostone, which differs from the host rocks (siliciclastic rocks) of the SEDEX-type. Moreover, the steeply VL has been discovered with the mining

exposures (Fig. 4), suggesting that the Maozu deposit has an epigenetic origin. Furthermore, George et al. (2015) found that galena from the SEDEX Pb-Zn deposit is enriched in Bi (>100 ppm, up to 1000 ppm), but Bi in galena from the Maozu deposit is normally below 1 ppm. In plots of Fe vs. Mn, Fe vs. Bi, Mn vs. Bi, and Ag vs. Bi (Fig. 11), the trace elements in galena of the Maozu deposit plot away from those of the SEDEX deposits (George et al. 2015, 2016; Ye et al. 2016). Therefore, we consider that the Maozu deposit is unlikely attributed to a syngenetic origin.

Previous studies have suggested that the Maozu deposit is characterized by: (1) stratiform and dipping vein ore bodies hosted in the Late Ediacaran Dengying Formation dolostone; (2) relatively simple mineral assemblage containing sphalerite, galena, dolomite, and minor pyrite and quartz; (3) ore-forming fluids with low-medium temperature (140–280 °C) and medium-high salinity (10–18 wt% NaCl eqv.) (Yang et al. 2017); (4) a mixing metal source of metamorphic basement rocks and ore-hosting sedimentary rocks (Zhou et al. 2013); and (5) sulfur from thermochemical reduction of the ore-hosting sulfate (Zhou et al. 2013). All these geological features are consistent with those of typical MVT deposits (Leach 1993, Sangster 1996; Leach et al. 2005, 2006; Leach and Taylor 2009).

Trace elements in sphalerite, such as Fe, Mn, Cd, Ge, In, Ga, Se, and Te, have been used to classify the deposit genesis in

recent decades because trace elements provide genetic information (Zhang 1987; Cook et al. 2009; Ye et al. 2011, 2012, 2016; Wei et al. 2018a, 2018b). In general, the MVT Pb-Zn deposit is enriched in Cd, Ge, and Ga (Ye et al. 2011; Bonnet et al. 2016; Yuan et al. 2018) and depleted in Fe, Mn, In, Sn, and Co (Ye et al. 2011, 2016; Wei et al. 2018a). The massive sulfide deposits (SEDEX and VMS) are characterized by enrichment in Fe, Mn, and In and depletion in Cd, Ge, and Ga (Cook et al. 2009; Ye et al. 2011; Wei et al. 2018b). The skarn-type deposits are enriched in Mn and Co and depleted in In, Sn, and Fe (Cook et al. 2009; Ye et al. 2011). For the Maozu deposit, trace-element compositions in sphalerite are characterized by depletion in Fe, Mn, and Co. The Mn and Co contents in sphalerite from the Maozu deposit are lower than that of the skarn-type (most of Mn >1000 ppm and Co >200 ppm, Supplemental¹ Table S1 (Cook et al. 2009; Ye et al. 2011)), and the Fe and Mn contents are significantly lower than those in the sedimentary exhalative deposit (most of Fe and Mn >1000 ppm, Supplemental¹ Table S1) (Ye et al. 2011). However, these sphalerite samples are enriched in Cd and Ge, which are analogous to those of MVT deposits from the U.S.A., China, and Mexico (Cook et al. 2009; Ye et al. 2011; Bonnet et al. 2016; Wei et al. 2018a). Furthermore, in the binary plots of different genesis deposits (Fig. 12), including Mn vs. Fe, Mn vs. Co, Mn vs. Ge, and Cd/Fe vs. Mn, all the samples fall into

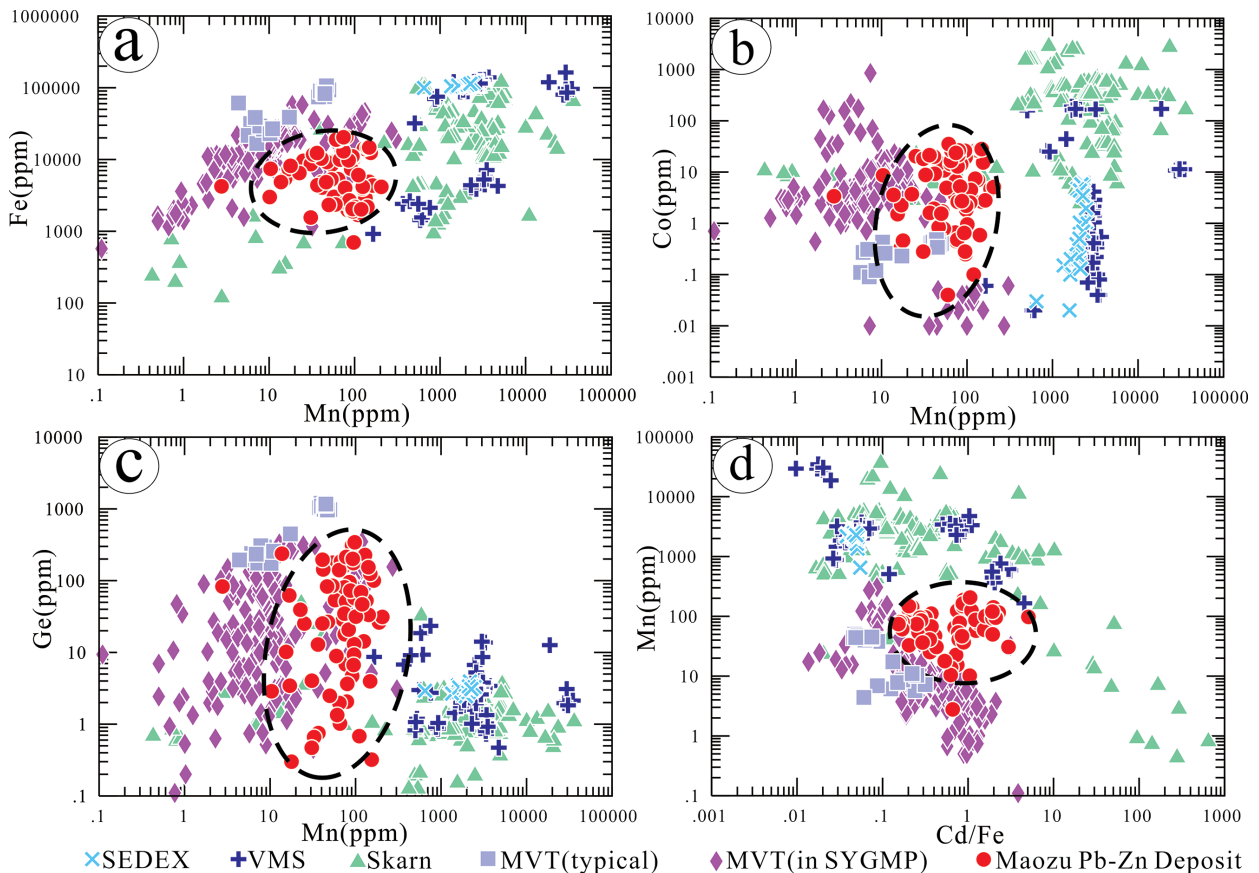


FIGURE 11. Binary plots of (a) Fe vs. Mn, (b) Fe vs. Bi, (c) Mn vs. Bi, and (d) Ag vs. Bi in galena from Maozu and other genesis Pb-Zn deposits [the data of SEDEX are from Ye et al. (2011) and George et al. (2015, 2016); the MVT data are from Ye et al. (2016)]. (Color online.)

the MVT range.

In conclusion, the composition of trace elements in sulfides from the Maozu Pb-Zn deposit is significantly different from that of the sedimentary exhalative and skarn-type deposits but consistent with that of the MVT deposits (Cook et al. 2009; Ye et al. 2011, 2016; Wei et al. 2018a, 2018b). Combined with the geological and geochemical characteristics of the deposit, we propose that the deposit is an MVT deposit.

A possible reason for the anomalies of Indium and Tin in sphalerite

Generally, the magma-related deposits show high In and Sn concentrations in sphalerite (e.g., Cook et al. 2009; Belissant et al. 2014; Wei et al. 2018b). Most of the Pb-Zn deposits in the SYGMP are considered as MVT that have no genetic relationship with igneous rock (Leach et al. 2005). Therefore, the concentrations of In and Sn in these deposits are very low (most <10 ppm, Fig. 6). However, several LA-ICP-MS spot analyses in this study display high concentrations of In and Sn. Interestingly, Mo et al. (2013) found that the volcanic rocks in the basement (the main metal source of these Pb-Zn deposits in the SYGMP) contain high levels of In (78 ppm) and Sn (120 ppm). Meanwhile, the mineralizing fluids of MVT deposits are defined as a long-distance migration

of basinal fluid (Garven 1985; Garven and Ruffensperger 1997). Therefore, a possible explanation is that the hydrothermal fluid flowed through the basement, including In-Sn-bearing volcanic rocks, and leached the metals out, which eventually formed as In-Sn-bearing sphalerite because In and Sn preferred host in sphalerite (Höll et al. 2007; Cook et al. 2009). But this hypothesis should be verified in the future.

IMPLICATIONS

To understand the genesis of Pb-Zn deposits in the SYGMP, the trace elements in different sulfides (sphalerite and galena) from the Maozu Pb-Zn deposit, which is a representative Pb-Zn deposit in the SYGMP, were analyzed by LA-ICP-MS. Compared with trace elements in sulfides from other genetic type Pb-Zn deposits, the Maozu Pb-Zn deposit is characterized by enrichment of Ge, Fe, Mn, Co in sphalerite and Ag, Sb, Cd, Se in galena, which is similar to the composition of typical MVT deposits and different from those of SEDEX, VMS, and skarn-type Pb-Zn deposits, suggesting that the Maozu deposit is an MVT deposit.

The occurrence of the trace elements in sulfides were determined by the LA-ICP-MS acquisition profiles, mapped images, and element inter-correlation. Bivalent cations such as Mn, Cd, Fe, and Co likely enter the sphalerite structure via a direct

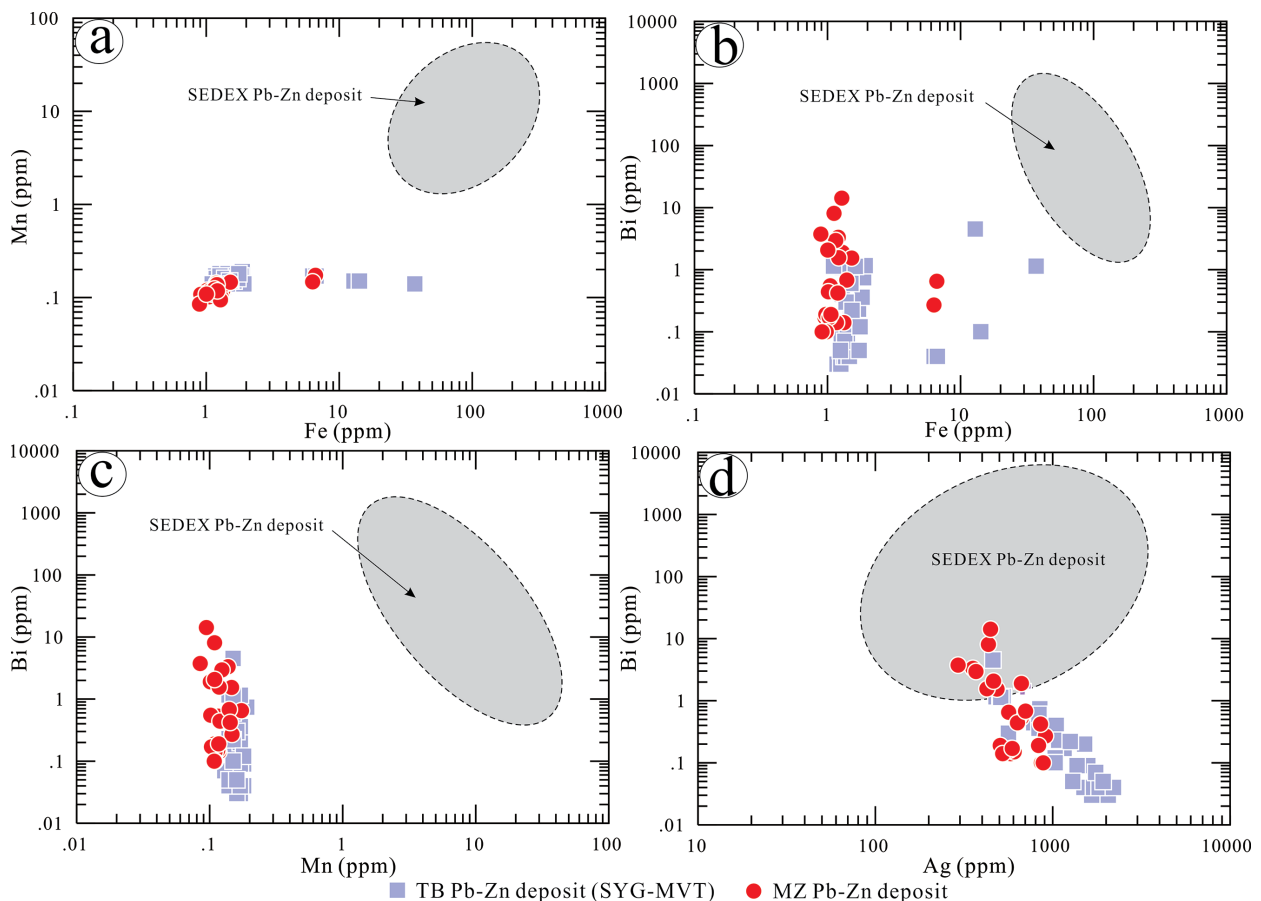


FIGURE 12. Binary plots of (a) Mn vs. Fe, (b) Mn vs. Co, (c) Mn vs. Ge, and (d) Cd/Fe vs. Mn in sphalerite from Maozu and other genesis Pb-Zn deposits [the data of other genesis deposits are from Cook et al. (2009), Ye et al. (2011, 2016), Li (2016), Yuan et al. (2018), and Wei et al. (2018a, 2018b)]. (Color online.)

substitution. Tri- and tetravalent elements including In^{3+} , Sn^{4+} , Ge^{4+} , and Sb^{3+} were incorporated into sphalerite by coupling with monovalent elements (Cu^+ , Ag^+) as $2\text{In}^{3+} + \text{Sn}^{4+} + 2\Box \leftrightarrow 5\text{Zn}^{2+}$ (\Box = vacancies) and $4(\text{Cu}^+ + \text{Sb}^{3+}) + (\text{Ge}^{4+} + 2\text{Ag}^+) + 2\Box \leftrightarrow 13\text{Zn}^{2+}$. Partly Pb and As exist in sphalerite as micro-inclusions. In addition, strong binary correlations between Sb and Ag in galena imply the coupled substitution of $\text{Ag}^+ + \text{Sb}^{3+} \leftrightarrow 2\text{Pb}^{2+}$.

The enrichment of trace elements in sulfide minerals differs among the lower layer (LL), vein layer (VL), and upper layer (UL). In sphalerite, Fe, Co, Cu, and Ge show a slight decrease trend while Cd, Mn, Ag, Sb, and Pb display a gradually increasing trend from the upper to lower layer. Notably, Fe, In, and Sn in sphalerite and Ag and Sb in galena are the highest in the VL, suggesting that the VL is a secondary migration channel of the ore-forming fluids.

ACKNOWLEDGMENTS AND FUNDING

We thank Ivan Belousov, Paul Olin, and Sarah Gilbert (CODES, University of Tasmania) for their assistance in LA-ICP-MS analysis. Associate Editor Daniel Gregory, and two anonymous reviewers are thanked for their constructive comments and suggestions. This research was jointly supported by the National Natural Science Foundation of China (Grant No. 41673056, 41430315), the National Key R&D Program of China (No. 2017YFC0602502), and the National "973 Project" (No. 2014CB440906).

REFERENCES CITED

- Alfantazi, A.M., and Moskalyk, R.R. (2003) Processing of indium: A review. *Minerals Engineering*, 16, 687–694.
- Belissant, R., Boiron, M.C., Luais, B., and Cathelineau, M. (2014) LA-ICP-MS analyses of minor and trace elements and bulk Ge isotopes in zoned Ge-rich sphalerites from the Noailhac–Saint-Salvy deposit (France): Insights into incorporation mechanisms and ore deposition processes. *Geochimica et Cosmochimica Acta*, 126, 518–540.
- Bernstein, L.R. (1985) Germanium geochemistry and mineralogy. *Geochimica et Cosmochimica Acta*, 49(11), 2409–2422.
- (1986) Geology and mineralogy of the APEX germanium–gallium mine, Washington County, Utah. U.S. Geological Survey Bulletin 1577, 1–9.
- Bonnet, J., Mosser, R.R., Caumon, M.C., Rouer, O., Andre, M.A.S., Cauzid, J., and Peiffert, C. (2016) Trace element distribution (Cu, Ga, Ge, Cd, and Fe) in sphalerite from the Tennessee Mvt deposits, U.S.A., by combined EMPA, LA-ICP-MS, Raman spectroscopy, and crystallography. *Canadian Mineralogist*, 54(5), 1261–1284.
- Cao, H.W., Zhang, S.T., Zheng, L., Liu, R.P., Tian, H.H., Zhang, X.H., and Li, J.J. (2014) Geochemical characteristics of trace element of sphalerite in the Zhongyuku (Pb)-Zn deposit of the Luanchuan, Southwest of China. *Mineral and Petrology*, 34(3), 50–59 (in Chinese with English abstract).
- Chen, Q.L. (2002) Metallogenic geological features and ore guides of high-grade Pb-Zn deposits in Yuhucun formation, northeast Yunnan. *Geology Prospecting*, 38(1), 22–26 (in Chinese with English abstract).
- Chutas, N.I., Kress, V.C., Ghiorsio, M.S., and Sack, R.O. (2008) A solution model for high temperature $\text{PbS-AgSbS}_2\text{-AgBiS}_2$ galena. *American Mineralogist*, 93, 1630–1640.
- Cook, N.J., Ciobanu, C.L., Pring, A., Skinner, W., Shimizu, M., Danyushevsky, L., Saini-Eidukat, B., and Melcher, F. (2009) Trace and minor elements in sphalerite: A LA-ICPMS study. *Geochimica et Cosmochimica Acta*, 73, 4761–4791.
- Cook, N.J., Ciobanu, C.L., Brugger, J., Etschmann, B., Howard, D.L., De Jonge, M.D., Ryan, C., and Paterson, D. (2012) Determination of the oxidation state of Cu in substituted CuIn-Fe-bearing sphalerite via I-XANES spectroscopy. *American Mineralogist*, 97, 476–479.
- Cook, N.J., Etschmann, B., Ciobanu, C.L., Geraki, K., Howard, D.L., Williams, T., Rae, N., Pring, A., Chen, G.R., Johannessen, B., and Brugger, J. (2015) Distribution and substitution mechanism of Ge in a Ge-(Fe)-bearing sphalerite. *Minerals*, 5(2), 117–132.
- Danyushevsky, L., Robinson, P., McGoldrick, P., Large, R., and Gilbert, S. (2003) LA-ICPMS of sulphides: evaluation of an XRF glass disc standard for analysis of different sulphide matrixes. *Geochimica et Cosmochimica Acta*, 67(18), A73.
- Danyushevsky, L., Robinson, P., Gilbert, S., Norman, M., Large, R., McGoldrick, P., and Shelley, M. (2011) Routine quantitative multi-element analysis of sulphide minerals by laser ablation ICP-MS: Standard development and consideration of matrix effects. *Geochemistry Exploration Environment Analysis*, 11(1), 51–60.
- Frenzel, M., Hirsch, T., and Gutzmer, J. (2016) Gallium, germanium, indium, and other trace and minor elements in sphalerite as a function of deposit type—A meta-analysis. *Ore Geology Reviews*, 76(9), 52–78.
- Gao, H.X., Ren, X.H., Guo, J., Li, F.R., and Li, X. (2011) Geological-geophysical characteristics and orebody prediction of Maozu lead-zinc deposit. *Mineral Resources and Geology*, 25(2), 152–157 (in Chinese with English abstract).
- Garven, G. (1985) The role of regional fluid flow in the genesis of the PinePoint deposit, western Canada sedimentary basin. *Economic Geology*, 80, 307–324.
- Garven, G., and Raffensperger, J.P. (1997) Hydrology and geochemistry of ore genesis in sedimentary basins. In H.L. Barnes, Ed., *Geochemistry of Hydrothermal Ore Deposits*, 3rd ed., 125–189. Wiley.
- George, L., Cook, N.J., Ciobanu, C.L., and Wade, B.P. (2015) Trace and minor elements in galena: A reconnaissance LA-ICP-MS study. *American Mineralogist*, 100(2–3), 548–569.
- George, L., Cook, N.J., and Ciobanu, C.L. (2016) Partitioning of trace elements in co-crystallized sphalerite–galena–chalcopyrite hydrothermal ores. *Ore Geology Reviews*, 77, 97–116.
- Gregory, D., Meffre, S., and Large, R. (2014) Comparison of metal enrichment in pyrite framboids from a metal-enriched and metal-poor estuary. *American Mineralogist*, 99, 633–644.
- Gregory, D.D., Large, R.R., Halpin, J.A., Baturina, E.L., Lyons, T.W., Wu, S., Danyushevsky, L., Sack, P.J., Chappaz, A., Maslennikov, V.V., and Bull, S.W. (2015) Trace element content of sedimentary pyrite in black shales. *Economic Geology*, 110, 1389–1410.
- Han, R.S., Liu, C.Q., Huang, Z.L., Chen, J., Ma, D.Y., Lei, L., and Ma, G.S. (2007) Geological features and origin of the Huize carbonate-hosted Zn-Pb-(Ag) District, Yunnan, South China. *Ore Geology Reviews*, 31, 360–383.
- He, S.H., Rong, H.H., Shang, W., and Su, J.H. (2006) Geological characteristics and genesis of Maozu lead and zinc deposit, Yunnan. *Mineral Resource Geology*, 4–5, 397–402 (in Chinese with English abstract).
- Höll, R., Kling, M., and Schroll, E. (2007) Metallogenesis of germanium—A review. *Ore Geology Reviews*, 30, 145–180.
- Hu, R.Z., and Zhou, M.F. (2012) Multiple Mesozoic mineralization events in South China—An introduction to the thematic issue. *Mineralium Deposita*, 47, 579–588.
- Huang, Z.L., Chen, J., Han, R.S., Li, W.B., Liu, C.Q., Zhang, Z.L., Ma, D.Y., Gao, D.R., and Yang, H.L. (2004) The ore geochemistry and its ore genesis of Huize super large scale Pb-Zn deposit-discussion on the relationship between Pb-Zn mineralization and Emeishan basalt, Beijing. *Geology Publishing Company Press*, 1–187 (in Chinese).
- Jeppsson, M.L. (1989) Mineral chemistry of silver in antimony and bismuth rich sulphide ore in Bergslagen, central Sweden. *Neues Jahrbuch für Mineralogie Monatshefte*, 205–216.
- Johan, Z. (1988) Indium and germanium in the structure of sphalerite: An example of coupled substitution with Copper. *Mineralogy and Petrology*, 39(3–4), 211–229.
- Kelley, K.D., Leach, D.L., Johnson, C.A., Clark, J.L., Fayek, M., Slack, J.F., Anderson, V.M., Ayuso, R.A., and Ridley, W.I. (2004) Textural, compositional, and sulfur isotope variations of sulfide minerals in the Red Dog Zn-Pb-Ag Deposits, Brooks Range, Alaska. Implications for Ore Formation. *Economic Geology*, 99(7), 1509–1532.
- Leach, D.L. (1993) Mississippi Valley-type lead-zinc deposits. *Geological Association of Canada Special Paper*, 40(3), 108–117.
- Leach, D.L., and Taylor, R.D. (2009) Mississippi Valley-type lead-zinc deposit model: U.S. Geological Survey Open-File Report, 1213, 5p.
- Leach, D.L., Sangster, D.F., Kelley, K.D., Large, R.R., Garven, G., Allen, C.R., Gutzmer, J., and Walters, S. (2005) Sediment-hosted lead-zinc deposits: A global perspective. *Economic Geology 100th Anniversary Volume*, 100, 561–607.
- Leach, D.L., Macquar, J.C., Lagneau, V., Leventhal, J., Emsbo, P., and Premo, W. (2006) Precipitation of lead-zinc ores in the Mississippi Valley type deposit at Trèves, Cévennes region of southern France. *Geofluids*, 6, 24–44.
- Li, Z.L. (2016) Geological geochemical characteristics and prospecting directions in the Fule lead-zinc deposit, Yunnan Province. Master thesis, Guiyang: Institute of Geochemistry, Chinese Academy of Sciences, 1–75 (in Chinese with English abstract).
- Li, Z.L., Ye, L., Hu, Y.S., and Huang, Z.L. (2018a) Geological significance of nickelerite minerals in the Fule Pb–Zn deposit, Yunnan Province, China. *Acta Geochimica*, 37(5), 684–690.
- Li, Z.L., Ye, L., Huang, Z.L., Nian, H.L., and Zhou, J.X. (2016) The primary researching on the trace elements in sphalerite in the Tianqiao Pb-Zn Deposit, Northwestern Guizhou. *ACTA Mineralogica Sinica*, 36(2), 183–188 (in Chinese with English abstract).
- Li, Z.L., Ye, L., Huang, Z.L., Zhou, J.X., Hu, Y.S., and Nian, H.L. (2018b) Mineralogical characteristics and geological significance of Copper minerals in Fule Pb-Zn deposit, Yunnan Province, China. *Geological Journal of China Universities*, 24(2), 200–209 (in Chinese with English abstract).
- Liu, W.Z. (2009) Geological and geochemical characteristics and metallogenic mechanism analysis of the Pb–Zn deposit in Maozu, Yunnan, China. *Journal of Chengdu University of Technology*, 36, 480–486 (in Chinese with English abstract).
- Liu, H.C., and Lin, W.D. (1999) Study on the law of Pb-Zn-Ag ore deposit in north-east Yunnan, China. *Yunnan University Press*, Kunming, 1–468 (in Chinese).
- Liu, H.T., and Zhang, Y.X. (2013) Study on leakage anomalies techniques of geo-

- chemical prospecting—Giving an example of Maozu Pb-Zn mining district, Qiaojia, Yunnan. *Mineral Resources and Geology*, 27(5), 403–408 (in Chinese with English abstract).
- Lueth, V.W., Megaw, P.K.M., Pingitore, N.E., and Goodell, P.C. (2000) Systematic variation in galena solid-solution compositions at Santa Eulalia, Chihuahua, Mexico. *Economic Geology*, 95, 1673–1687.
- Mladenova, V., and Valchev, S. (1998) Ga/Ge ratio in sphalerite from the carbonate-hosted Sedmochislenski Deposit as a temperature indication of initial fluids. *Review of the Bulgarian Geological Society*, 59(2–3), 49–54.
- Mo, X.Y., Chen, T.Y., He, L.T., Jiang, S.D., Zhang, Y.C., and Yang, C. (2013) The Kunyang group in Dongchuan, Yunnan, China. Kunming: Yunnan Science and Technology Press, 1–168 (in Chinese).
- Möller, P. (1987) Correlation of homogenization temperatures of accessory minerals from sphalerite-bearing deposits and Ga/Ge model temperatures. *Chemical Geology*, 61, 153–159.
- Moskalyk, R.R. (2003) Gallium: The backbone of the electronics industry. *Minerals Engineering*, 16, 921–929.
- Oftedal, I. (1940) Untersuchungen über die Nebenbestandteile von Erzmineralien norwegischer zinkblendführender Vorkommen. *Skrift. Norsk Vidensk. Akad. Oslo, Matematik-Naturvidenskab Kl.*, 8, 1–103.
- Renock, D., and Becker, U. (2011) A first principles study of coupled substitution in galena. *Ore Geology Reviews*, 42, 71–83.
- Sangster, D.F. (1996) Mississippi Valley-type lead-zinc. *Geology of Canadian Mineral Deposit Types: Geological Survey of Canada. Geology of Canada*, (8), 253–261.
- Tu, G.C. (1984) *Geochemistry of Strata-bound Ore Deposits in China (Volumes I)*. Science Press, Beijing, 13–69 (in Chinese with English abstract).
- Van Hook, H.J. (1960) The ternary system $Ag_2S-Bi_2S_3-PbS$. *Economic Geology*, 55, 759–788.
- Watling, R.J., Herbert, H.K., Barrow, I.S., and Thomas, A.G. (1995) Analysis of diamonds and indicator minerals for diamond exploration by laser ablation/inductively coupled plasma mass spectrometry. *Analyst*, 120(5), 1357–1364.
- Wei, A., Xue, C., Xiang, K., Li, J., Liao, C., and Akhter, Q.J. (2015) The ore-forming process of the Maoping Pb–Zn deposit, Northeastern Yunnan, China: Constraints from cathodoluminescence (CL) petrography of hydrothermal dolomite. *Ore Geology Reviews*, 70, 562–577.
- Wei, C., Huang, Z.L., Yan, Z.F., Hu, Y.S., and Ye, L. (2018a) Trace element contents in sphalerite from the Nayongzhi Zn–Pb Deposit, Northwestern Guizhou, China. *Minerals*, 8(11), 490–512.
- Wei, C., Ye, L., Huang, Z.L., Gao, W., Hu, Y.S., Li, Z.L., and Zhang, J.W. (2018b) Ore genesis and geodynamic setting of Laochang Ag–Pb–Zn–Cu Deposit, Southern Sanjiang Tethys Metallogenic Belt, China: Constraints from whole rock geochemistry, trace elements in sphalerite, zircon U–Pb dating and Pb isotopes. *Minerals*, 8(11), 516–544.
- Wei, C., Ye, L., Hu, Y.S., Danyushevskiy, L., Li, Z.L., and Huang, Z.L. (2019) A distribution and occurrence of Ge and related trace elements in sphalerite from the Lehong carbonate-hosted Zn–Pb deposit, northeastern Yunnan, China: Insights from SEM and LA-ICP-MS studies. *Ore Geology Reviews*. <https://doi.org/10.1016/j.oregeorev.2019.103175>.
- Wu, Y. (2013) The age and ore-forming process of MVT deposits in the boundary area of Sichuan–Yunnan–Guizhou provinces, Southwest China. Ph.D. thesis, China University of Geosciences, Beijing, 1–167 (in Chinese with English abstract).
- Xie, J.R. (1963) Introduction of the Chinese Ore Deposit. Academic books and periodicals publishing house, Beijing, 1–71 (in Chinese).
- Yang, Q., Zhang, J., Wang, J., Zhong, W.B., and Liu W.H. (2017) Study of ore-forming fluid geochemistry of Maozu large-scale lead-zinc deposit in northeast Yunnan. *Mineral Resources and Geology*, 31(5), 854–863 (in Chinese with English abstract).
- Ye, L., Cook, N.J., Ciobanu, C.L., Liu, Y.P., Zhang, Q., Liu, T.G., Gao, W., Yang, Y.L., and Danyushevskiy, L. (2011) Trace and minor elements in sphalerite from base metal deposits in South China: A LA-ICPMS study. *Ore Geology Reviews*, 39, 188–217.
- Ye, L., Gao, W., Yang, Y.L., Liu, T.G., and Peng, S.S. (2012) Trace elements in sphalerite in Laochang Pb–Zn polymetallic deposit, Lancang, Yunnan Province. *Acta Petrologica Sinica*, 28(5), 1362–1372 (in Chinese with English abstract).
- Ye, L., Li, Z.L., Hu, Y.S., Huang, Z.L., Zhou, J.X., Fan, H.F., and Danyushevskiy, L. (2016) Trace elements in sulfide from the Tianbaoshan Pb–Zn deposit, Sichuan Province, China: A LA-ICPMS study. *Acta Petrologica Sinica*, 32(11), 3377–3393 (in Chinese with English abstract).
- Yuan, B., Zhang, C.Q., Yu, H.J., Yang, Y.M., Zhao, Y.X., Zhu, C.C., Ding, Q.F., Zhou, Y.B., Yang, J.C., and Xu, Y. (2018) Element enrichment characteristics: insights from element geochemistry of sphalerite in Daliangzi Pb–Zn deposit, Sichuan, Southwest China. *Journal of Geochemical Exploration*, 186, 187–201.
- Zhang, C.Q. (2008) The genetic model of Mississippi Valley-type deposits in the boundary area of Sichuan, Yunnan and Guizhou province, China. Ph. D. Dissertation. Beijing, China University of Geosciences, 1–167 (in Chinese with English abstract).
- Zhang, C.Q., Mao, J.W., Wu, S.P., Liu, F., Guo, B.J., and Gao, D.R. (2005) Distribution, characteristics and genesis of Mississippi Valley Type lead-zinc deposits in Sichuan–Yunnan–Guizhou area. *Mineral Deposits*, 24(3), 336–348 (in Chinese with English abstract).
- Zhang, C.Q., Wu, Y., Hou, L., and Mao, J.W. (2015) Geodynamic setting of mineralization of Mississippi Valley-type deposits in world-class Sichuan–Yunnan–Guizhou Zn–Pb triangle, southwest China: Implications from age-dating studies in the past decade and the Sm–Nd age of Jinshachang deposit. *Journal of Asian Earth Sciences*, 103, 103–114.
- Zhang, Q. (1987) Trace elements in galena and sphalerite and their geochemical significance in distinguishing the genetic types of Pb–Zn ore deposits. *Chinese Journal of Geochemistry*, 6, 177–190.
- Zhang, R.W. (2013) Geochemical characteristics and genetic type of the Maozu Pb–Zn deposit in Yunnan province, China. Kunming University of Science and Technology, 1–82 (in Chinese with English abstract).
- Zhang, W.J. (1984) The sedimentary genesis and metallogenic rules of Pb–Zn deposits in northeast Yunnan province. *Geology and Exploration*, 7, 11–16 (in Chinese).
- Zhang, Z.B., Li, C.Y., Tu, G.C., Xia, B., and Wei, Z.Q. (2006) Geotectonic evolution background and ore-forming process of Pb–Zn deposits in Chuan–Dian–Qian area of Southwest China. *Geotectonica et Metallogenia*, 30(3), 343–354 (in Chinese with English abstract).
- Zhou, J.X., Huang, Z.L., and Yan, Z.F. (2013) The origin of the Maozu carbonate-hosted Pb–Zn deposit, southwest China: Constrained by C–O–S–Pb isotopic compositions and Sm–Nd isotopic age. *Journal of Asian Earth Sciences*, 73, 39–47.
- Zhou, J.X., Luo, K., Wang, X.C., Wilde, S.A., Wu, T., Huang, Z.L., Cui, Y.L., and Zhao, J.X. (2018a) Ore genesis of the Fule Pb–Zn deposit and its relationship with the Emeishan Large Igneous Province: Evidence from mineralogy, bulk C–O–S and in situ S–Pb isotopes. *Gondwana Research*, 54, 161–179.
- Zhou, J.X., Xiang, Z.Z., Zhou, M.F., Feng, Y.X., Luo, K., Huang, Z.L., and Wu, T. (2018b) The giant Upper Yangtze Pb–Zn province in SW China: Reviews, new advances and a new genetic model. *Journal of Asian Earth Sciences*, 154, 280–315.
- Zhu, C.W., Wen, H.J., Zhang, Y.X., Fu, S.H., Fan, H.F., and Cloquet, C. (2016) Cadmium isotope fractionation in the Fule Mississippi Valley-type deposit, Southwest China. *Mineralium Deposita*, 52, 675–686.

MANUSCRIPT RECEIVED JANUARY 5, 2019

MANUSCRIPT ACCEPTED APRIL 24, 2020

MANUSCRIPT HANDLED BY DANIEL GREGORY

Endnote:

¹Deposit item AM-20-116950, Supplemental Material. Deposit items are free to all readers and found on the MSA website, via the specific issue's Table of Contents (go to http://www.minsocam.org/MSA/AmMin/TOC/2020/Nov2020_data/Nov2020_data.html).